Endogenous RALF peptide function is required for powdery mildew host colonization

Henriette Leicher[1], Sebastian Schade[1,#], Jan W. Huebbers[2], Kristina S. Munzert-Eberlein[3], Genc Haljiti[4], Christina Ludwig[4], Marion Müller[1], Toshinori Kinoshita[5,6], Timo Engelsdorf[3], Ralph Hückelhoven[1] and Martin Stegmann[1,#]

[1]Chair of Phytopathology, TUM School of Life Sciences, Technical University of Munich, Freising, Germany

[2]Unit of Plant Molecular Cell Biology, Institute for Biology I, RWTH Aachen University, Aachen, Germany

[3]Molecular Plant Physiology, Department of Biology, Philipps-Universität Marburg, Marburg, Germany

[4]Bavarian Center for Biomolecular Mass Spectrometry (BayBioMS), TUM School of Life Science, Technical University of Munich (TUM), Freising, Germany

[5]Graduate School of Science, Nagoya University, Chikusa, Nagoya, Japan

[6]Institute of Transformative Bio-Molecules (WPI-ITbM), Nagoya University, Chikusa, Nagoya, Japan

[#]present address: Institute of Botany, Molecular Botany, Ulm University, Germany

*Corresponding author: Email: martin.stegmann@tum.de

Abstract

The receptor kinase FERONIA (FER) is a susceptibility factor for biotrophic powdery mildew fungal pathogens in *Arabidopsis thaliana*, but the underlying molecular mechanisms remain largely unknown. FER is required for the perception of endogenous RAPID ALKALINIZATION FACTOR (RALF) peptides to control various aspects of plant growth, development and immunity. RALFs are perceived by FER-LORELEI-LIKE GPI-ANCHORED PROTEIN (LLG) heterocomplexes to induce cellular responses and bind to LEUCINE-RICH REPEAT EXTENSIN (LRX) proteins as structural components of the cell wall. We show that FER`s RALF ligands are necessary for full success of powdery mildew colonization. Our data reveals that LLGs and LRXs are also powdery mildew susceptibility factors, and that the susceptibility function of RALFs is best explained by a combination of peptide signalling and cell wall-related effects. We further reveal that cell wall and apoplastic pH homeostasis, hallmark features of RALF function, support powdery mildew reproductive success. The function of host RALF peptides is underlined by the fact that, in contrast to previously described pathogens that hijack FER for colonization, powdery mildew fungi do not produce functional RALF mimics. Surprisingly, RALF-dependent powdery mildew pathogenesis is partially independent of FER. The resistance phenotype of *ralf* and *fer* mutants is not associated with de-regulated salicylic acid and jasmonic acid signalling, important defense-related phytohormones. Collectively, powdery mildew fungi require RALF signalling for apoplastic pH regulation and cell wall structural organization for successful colonization, highlighting a novel mechanism for host susceptibility by obligate biotrophic fungi.

Key words: RALF peptides, powdery mildew, FER, peptide signalling, cell wall, pH homeostasis

41 **Introduction**

42 Plants have evolved a multi-layered immune system to defend against potential pathogens. Pattern-
43 triggered immunity (PTI) is activated through the perception of conserved microbe-derived molecular
44 signatures (microbe-associated molecular patterns, MAMPs) or host derived damage-associated
45 molecular patterns (DAMPs) by plasma membrane localized pattern recognition receptors (PRRs),
46 which are either receptor-like kinases (RLKs) or receptor-like proteins (RLPs). To subvert PTI, host
47 adapted pathogens evolved effectors that again can be perceived by specific resistance (R) proteins
48 (encoded by R-genes) including intracellular localized nucleotide-binding leucine-rich repeat receptors
49 (NB-LRRs). Effector recognition activates a strong second layer of immunity culminating in the
50 hypersensitive response (HR) involving cell death to inhibit proliferation of biotrophic pathogens (Ngou
51 et al., 2022) .

52 Other genetic factors affecting infection success are susceptibility genes (S-genes). These encode plant
53 factors with various endogenous functions that can be utilized by pathogens for their own benefit. In
54 consequence, mutating S-genes usually confers pathogen genotype-independent and hence durable
55 disease resistance (Engelhardt et al., 2018; van Schie and Takken, 2014).

56 With over 400 different species that infect nearly 10 000 possible host plants, powdery mildew is one of
57 the most widespread fungal plant diseases, also affecting a variety of economically relevant crop species
58 (Glawe, 2008). During the powdery mildew infection cycle, a continuous interaction occurs between the
59 obligate biotrophic fungus and its host plant, which determines the infection success at multiple levels.
60 The first well-characterized powdery mildew susceptibility factor is the barley MILDEW LOCUS O (MLO)
61 protein, that confers barley susceptibility towards adapted *Blumeria hordei*. The *mlo* mutants show race-
62 unspecific resistance against powdery mildew even after decades of field application. Mutants in *mlo*
63 are powdery mildew resistant in phylogenetically diverse plant species, including *Arabidopsis* and
64 tomato, suggesting that *S*-genes are functionally conserved (Kusch and Panstruga, 2017).
65 In addition to their function as PRRs, RLKs are important sensors for endogenous signals regulating
66 growth and/or modulating immunity (Rzemieniewski and Stegmann, 2022). Adapted pathogens can
67 hijack these RLK pathways to facilitate successful host accommodation. In *Arabidopsis*, IMPAIRED
68 OOMYCETE SUSCEPTIBILITY 1 (IOS1) and SYMRK-HOMOLOGOUES RKs (ShRKs) are
69 susceptibility factors for *Hyaloperonospora arabidopsidis* (*Hpa*) infection but they show mild or no
70 susceptibility function in interaction with the powdery mildew fungus *Erysiphe cruciferarum* (Hok et al.,
71 2014; Hok et al., 2011; Ried et al., 2019). Silencing of specific powdery mildew infection-regulated RLKs
72 enhances penetration resistance to *Blumeria hordei* (*Bh*) in single cell transformation experiments
73 (Douchkov et al., 2014; Schnepf et al., 2018).

74 The RLK FERONIA (FER) is an important regulator of diverse physiological responses. FER and related
75 CATHARANTUS ROSEUS RECEPTOR-LIKE KINASE 1-LIKEs (CrRLK1Ls) perceive endogenous
76 RAPID ALKALINIZATION FACTOR (RALF) peptides to regulate multiple plant processes, including
77 pollen hydration, pollen tube growth, polytubey block, intergeneric hybridization and root hair growth (Ge
78 et al., 2017; Gonneau et al., 2018; Lan et al., 2023; Zhong et al., 2022; Zhu et al., 2021). FER contributes
79 to PTI by acting as a RALF-regulated scaffold protein for PRR complexes (Stegmann et al., 2017). FER
80 perceives RALF peptides in a heteromeric complex with the GPI anchored protein LORELEI-LIKE GPI

81 ANCHORED PROTEIN 1 (LLG1) (Li et al., 2015; Xiao et al., 2019). In controlling antibacterial
82 resistance, FER´s role is associated with a function in jasmonic acid (JA) signalling. Here, FER
83 phosphorylates and destabilize the JA downstream transcription factor MYELOCYTOMATOSIS 2
84 (MYC2) to enhance resistance to *Pseudomonas syringae* pv. *tomato* (*Pto*) (Guo et al., 2018). RALF
85 peptides also bind to LRX proteins but the biochemical interplay between LRX and FER-LLG complexes
86 remains little understood (Dünser et al., 2019; Gronnier et al., 2022; Mecchia et al., 2017; Moussu et al.,
87 2020; Zhao et al., 2018). Recent reports show that RALF peptides (via binding to LRXs) have a structural
88 role in organizing the patterning of demethylesterified pectins in the cell wall. This suggests that pectin
89 may connect cell wall structural LRX-RALF complexes with plasma membrane-localized CrRLK1Ls that
90 in turn monitor cell wall integrity (Moussu et al., 2023; Schoenaers et al., 2024). The central role of FER-
91 LLG/LRX-RALF modules for plant physiology is highlighted by the fact that adapted pathogens can
92 hijack RALF signalling for their own benefit. *Fusarium oxysporum* and root knot nematodes produce a
93 RALF mimic to enhance infection success on tomato and *Arabidopsis* (Masachis et al., 2016; Thynne
94 et al., 2017; Zhang et al., 2020). This function is likely related to RALF-mediated immune suppression
95 and physiological reprogramming. Furthermore, the *fer-1* mutant in the Ler-0 *Arabidopsis* ecotype is less
96 susceptible to the powdery mildew disease caused by *Erysiphe orontii*, suggesting that FER acts as an
97 *S*-factor for powdery mildew (Kessler et al., 2010). Yet, how FER confers susceptibility remains little
98 understood.

99 Here, we sought out to unravel the molecular mechanism of FER-mediated powdery mildew
100 susceptibility. We confirmed FER`s function in powdery mildew colonization in the Col-0 *fer-4* mutant
101 using the adapted Arabidopsis-infecting powdery mildew species *Erysiphe cruciferarum*. We show that
102 other RALF binding and receptor complex-related proteins, including LLGs and LRX, are required for
103 successful *Ecr* colonization. By loss of function studies, we unravel RALF peptides as important
104 susceptibility factors for powdery mildew. CRISPR Cas9-generated *ralf22/23/33* (CRISPR *ralf3x*) and
105 *ralf1/18/22/23/31/33/34 (*CRISPR *ralf7x)* show increasing resistance to powdery mildew infection
106 depending on the number of eliminated RALFs. Our bioinformatic analysis suggests that powdery
107 mildew fungi do not encode functional RALF peptide mimics, supporting that mildew requires host-
108 endogenous RALF signalling for its own benefit (Masachis et al., 2016; Thynne et al., 2017). We suggest
109 that the enhanced resistance of *fer* and CRISPR *ralf7x* is not associated with defects in MLO-mediated
110 fungal penetration or deregulation of defense-related phytohormone signalling. Instead, powdery mildew
111 might require FER-RALF-mediated apoplastic pH regulation and cell wall remodelling for successful
112 colonization. Surprisingly, our data indicates that RALF-mediated powdery mildew susceptibility is only
113 partially dependent on FER and exerts its effect in a combination of signalling and structural functions.
114 We propose that powdery mildew fungi require RALFs to provide a favourable growth environment,
115 highlighting a novel mechanism of host subversion by adapted plant pathogens.

116 **Results**

117 **FER, LLGs and LRX are powdery mildew susceptibility factors**

118 The Ler-0 *fer-1* mutant was demonstrated to be more resistant to infection with the powdery mildew
119 species *Golovinomyces orontii* (Kessler et al., 2010). We confirmed this phenotype in the Arabidopsis

120 Col-0 ecotype using the well described *fer-4* mutant allele (Duan et al., 2010) and the powdery mildew
121 species *Erysiphe cruciferarum* (*Ecr*), which is also able to infect Arabidopsis (Micali et al., 2008).
122 Macroscopically the *fer-4* mutant showed slightly reduced visible disease symptoms compared to Col-0
123 (Fig. 1A). We quantified the resistance by counting conidiophores (the asexual reproductive structures
124 of this fungus) of individual colonies 5 days post *Ecr* inoculation. The *fer-4* mutant showed strongly
125 reduced conidiophore production compared to the WT control (Fig. 1B, C). Further quantification by
126 qPCR of relative fungal DNA, normalized to plant DNA, demonstrated reduced fungal growth on *fer-4*
127 (Fig. S1A). Expression of FER-GFP under the control of its native promoter complemented the
128 resistance phenotype of *fer-4* (Fig. 1C). This data indicates that *fer* loss of function mutants, across
129 ecotypes and fungal species, are more resistant to powdery mildew infection.

130 Next, we investigated whether FER-related RALF receptor complex components are involved in
131 powdery mildew susceptibility. We tested a loss of function mutant in the RALF receptor LLG1 (*llg1-2*)
132 which showed reduced conidiophore production (Fig. 1D). A similar effect was observed in the *llg1-3*
133 allele, in which LLG1 is impaired in RALF binding but mutants do not show *fer*-like growth phenotypes
134 (Fig. 1D, Fig. S8) (Shen et al., 2017). The resistance phenotype of the *llg1* mutants, however, was not
135 clear in qPCR quantification (Fig. S1B). Since qPCR gives an average infection level over the whole
136 plant, this method is more prone to uncontrollable differences in infection densities and is less sensitive
137 to mild phenotypes, unlike conidiophore counting, which evaluates the reproductive success of
138 individual colonies. Surprisingly, *llg1-2* and *llg1-3* were both previously described to be more susceptible
139 to the powdery mildew species *Golonivomyces cichoracearum* (Shen et al., 2017), raising the question
140 of mildew-species-dependent differences in *llg1* pathophenotypes, unlike *fer* (Fig. 1) (Kessler et al.,
141 2010) and potential redundancy of LLG1 with related members of the LRE/LLG gene family (Noble et
142 al., 2022; Xiao et al., 2019). Both *LLG2* and *LLG3* show very weak predicted expression in leaves (Xiao
143 et al., 2019), which does not exclude a role in leaf-related immune responses, as previously described
144 for the CrRLK1L ANXUR1 (Mang et al., 2017). In addition to the plasma membrane localized FER-LLG1
145 receptor complex, RALF peptides bind to cell wall localized LRX proteins with high affinity (Moussu et
146 al., 2020). A *lrx3 lrx4 lrx5* (*lrx3/4/5*) triple mutant phenocopies *fer* in immune signalling, salt stress
147 responses and overall plant morphology (Dünser et al., 2019; Gronnier et al., 2022; Moussu et al., 2020;
148 Zhao et al., 2018). This *lrx3/4/5* mutant displayed reduced conidiophore production upon *Ecr* infection
149 (Fig. 1E). Yet, the mutant did not show reduced relative fungal DNA content (Fig. S1C). Further mutating
150 *LRX1* and *LRX2* in *lrx3/4/5* (*lrx1/2/3/4/5*, hereafter referred to as *lrx5x* mutant) (Herger et al., 2020)
151 promoted the enhanced resistance phenotype (Fig. 1E, Fig. S1C). Altered plant morphology and PTI
152 responses of *lrx3/4/5* are indistinguishable from those in *fer-4* (Gronnier et al., 2022; Zhao et al., 2018),
153 suggesting that LRXs display an increased level of redundancy in the context of powdery mildew
154 susceptibility control. Overexpression of LRR4-citrine (LRX4 lacking the extensin domain) has a
155 dominant negative effect on plant growth, while PTI responses are not affected (Dünser et al., 2019;
156 Gronnier et al., 2022). The p35S::LRR4-citrine lines phenocopied *lrx5x* mutants and *fer-4* in showing
157 enhanced powdery mildew resistance (Fig. 1F).

158 **Powdery mildew requires endogenous RALF peptides for successful colonization**

159 Given the involvement of FER-LLG1 and LRXs in the establishment of powdery mildew pathogenesis
160 on Col-0, we hypothesized that RALF peptide signalling through FER-LLG1 and/or their binding to LRXs
161 is required for powdery mildew colonization. Many plant pathogens, including fungi, secrete functional
162 RALF peptide mimics to suppress immunity or reprogram host physiology (Masachis et al., 2016;
163 Thynne et al., 2017; Zhang et al., 2020). We searched available genomes of powdery mildew species
164 for the presence of potential RALF peptide mimics. However, consistent with previous reports (Thynne
165 et al., 2017) we could not detect evidence for RALF peptide mimics among different species of the order
166 *Erysiphales* (Table S1, method section for details on our bioinformatic search pipeline). Based on this,
167 we hypothesized that endogenous RALFs are involved in the *Ecr*-Arabidopsis interaction. To test this
168 hypothesis, we generated CRISPR mutants of leaf-expressed RALF peptides. The Arabidopsis genome
169 encodes for at least 37 RALF members (Abarca et al., 2021). We anticipated genetic redundancy and
170 generated CRISPR mutants in which we targeted *RALF23*, a well-described ligand of FER-LLG1
171 (Stegmann et al., 2017; Tang et al., 2022; Xiao et al., 2019) and seven additional RALF-peptides with
172 structural similarity to RALF23 and predicted leaf expression (*RALF1*, *RALF14*, *RALF18*, *RALF22*,
173 *RALF33*, *RALF23*, *RALF31*, *RALF34*) (Fig. S2A). We could not obtain an octuple mutant, raising the
174 question whether loss of multiple RALFs may cause severe developmental defects and/or lethality.
175 Nevertheless, two higher order mutants, a knockout of *ralf22/23/33* (hereafter CRISPR *ralf3x*) and a
176 *ralf1/18/22/23/31/33/34* mutant (hereafter CRISPR *ralf7x*) (Fig. 2A, Fig. S2B, C), were generated. While
177 the CRISPR *ralf3x* mutant only displayed a mild growth phenotype with slightly shortened petioles, the
178 CRISPR *ralf7x* mutant was strongly impaired in shoot growth (Fig. 2B, Fig. S2D, S8). Compared to *fer-*
179 *4*, however, CRISPR *ralf7x* showed less pronounced shoot growth defects with a trend towards longer
180 petioles (Fig. S2D) and an overall more wildtype-like morphology (Fig. 2B, Fig. S8). Interestingly, the
181 powdery mildew infection success was significantly reduced on CRISPR *ralf3x* and CRISPR *ralf7x*,
182 demonstrated by both a reduced number of conidiophores and decreased relative fungal DNA contents
183 (Fig. 2B-E). Importantly, CRISPR *ralf7x* displayed elevated resistance compared to *fer-4* (Fig. 2D, E).
184 Expression of p35S::RALF23 complemented the CRISPR *ralf7x* growth and powdery mildew infection
185 phenotype (Fig. 2F, Fig. S2E, S8). We also observed a strong powdery mildew resistance phenotype
186 with the previously reported *ralf1/22/23/31* quadruple mutant (Fig. 2G) (Lan et al., 2023). Collectively,
187 this data show that multiple FER-LLG1 and LRX-binding RALFs genetically contribute to powdery
188 mildew pathogenesis.

189 **FER and RALF mutants show post-penetration powdery mildew resistance**

190 We next sought out to unravel the cellular mechanism underlying RALF-mediated powdery mildew
191 susceptibility. Recent evidence showed that RALF-induced calcium influx in synergid cells and pollen
192 tubes is facilitated by FER-LRE-mediated activation of the NTA/MLO7 calcium channel (Gao et al.,
193 2022). The MLO family encodes for important powdery mildew susceptibility factors across different
194 families (Acevedo-Garcia et al., 2017; Büschges et al., 1997; Engelhardt et al., 2018; Li et al., 2022b;
195 Nekrasov et al., 2017; van Schie and Takken, 2014). In Arabidopsis, mutation of three partially
196 redundant MLOs is required to confer full penetration resistance (Consonni et al., 2006). Genetically,
197 MLO2 is the main susceptibility factor and active as a calcium channel in COS7 cell culture (Consonni

198 et al., 2006; Gao et al., 2022). This raises the possibility that RALF perception by FER-LLG complexes
199 activates MLO channels to facilitate mildew colonization.

200 MLO-YFP in barley and MLO2-GFP in Arabidopsis focally accumulate at powdery mildew penetration
201 sites (Bhat et al., 2005; Huebbers et al., 2024). MLO2 localization to the fungal penetration site was
202 confirmed with p35S::MLO2-mCherry lines (Fig. 3A, left panel). Further, we tested whether FER-GFP
203 accumulates at *Ecr* penetration sites using *fer-4 pFER::FER-GFP* (Duan et al., 2010). The FER-GFP
204 signal outlined the plasma membrane, but specific recruitment to the site of fungal attack, haustorial
205 neck and/or extrahaustorial membrane could not be detected (Fig. 3A, right panel). The *fer-4* mutant
206 shows strongly reduced production of conidiophores on infected tissue (Fig. 1C), but initial hyphal growth
207 is largely unaffected (Fig. 3B). This prompted us to assess whether *fer-4* or CRISPR *ralf7x* mutants
208 show any defect in epidermal cell penetration. Host cell entry by *Ecr* was successful in ~80% of
209 penetration attempts on Col-0. Surprisingly, we did not observe any difference in epidermal cell entry in
210 *fer-4* and CRISPR *ralf7x*. As previously reported (Consonni et al., 2006), the *mlo2/6/12* mutant showed
211 complete penetration resistance (Fig. 3C). This suggests that mutating RALF-related components
212 primarily affects reproductive success and not epiphytic growth, which may explain the overall milder
213 phenotypes we observed in qPCR-based quantification of *Ecr* infection success.

214 While callose deposition is mostly confined on Col-0 trichomes, the *mlo2/6/12* mutant displays aberrant
215 callose deposition in trichomes with delocalized or absent accumulation (Huebbers et al., 2024).
216 Likewise, *fer-4* mutants are impaired in trichome formation (Duan et al., 2010) which prompted us to test
217 whether *fer-4*, CRISPR *ralf7x* and *mlo2/6/12* show phenotypic similarities. We observed less trichomes
218 on *fer-4*, while the number of trichomes on CRISPR *ralf7x* was not significantly reduced (Fig. 3D).
219 Further, trichomes on *fer-4* tended to have fewer branches than trichomes on Col-0 while trichomes on
220 CRISPR *ralf7x* had more branches (Fig. 3E). Moreover, a fraction of trichomes on the CRISPR *ralf7x*
221 mutant were enlarged in the base region (≈ 22 %), which was not observed on Col-0 and *fer*-4 (Fig. 3F).
222 Unlike *mlo2/6/12*, neither CRISPR *ralf7x* nor *fer*-4 showed mis-regulated callose deposition in trichomes
223 (Fig. 3F)(Huebbers et al., 2024). Collectively, this data suggests that FER-RALF-dependent powdery
224 mildew susceptibility and trichome development is not directly linked to MLO function. Our data suggests
225 that mutation in FER-RALF primarily affects post-penetration fungal colonization.

226 **The powdery mildew resistance phenotype of *fer-4* is not associated with de-regulated salicylic**
227 **acid and jasmonic acid signalling**

228 Salicylic acid (SA) is an important defence hormone promoting resistance to biotrophic and
229 hemibiotrophic pathogens (Peng et al., 2021). For example, reduced powdery mildew colonization in
230 *POWDERY MILDEW RESISTANCE 4* (*PMR4*) mutants is dependent on enhanced SA signalling and
231 expression of the SA hydrolysing enzyme NahG enhances powdery mildew colonization (Nishimura et
232 al., 2003). Ler-0 *fer-1* seedlings did not show elevated *PATHOGENESIS-RELATED 1* (*PR1*) expression,
233 a marker gene of the SA pathway (Kessler et al., 2010). Yet, the weak *fer-5* allele in Col-0 (Duan et al.,
234 2010) showed mildly elevated SA levels in seedlings (Engelsdorf et al., 2018), prompting us to test
235 whether the mildew resistance phenotype in *fer-4* may be associated with elevated SA levels. We
236 quantified free and glycosylated SA by high pressure liquid chromatography (HPLC) upon *Ecr* infection.

237 As expected *Ecr* infection led to mildly enhanced levels of SA (Fig. 4A). However, neither *fer-4* nor
238 CRISPR *ralf7x* showed higher SA levels in the untreated state or after infection (Fig. 4A). We also
239 measured the major catabolic SA products 2,3-DHBA and 2,5-DHBA to investigate the flux through the
240 SA pathway (Zhang et al., 2013; Zhang et al., 2017) as well as camalexin levels, an indole alkaloid
241 associated with anti-fungal resistance (Liu et al., 2016; Mucha et al., 2019). Neither of those compounds
242 were significantly enhanced before or after infection in *fer-4* and CRISPR *ralf7x* compared to the Col-0
243 control (Fig. 4B, C, Fig. S3A). In accordance with the measured SA levels, *PR1* expression was not
244 elevated in any of the tested mutants in control conditions. *Ecr* infection resulted in enhanced *PR1*
245 expression levels which was observed in all tested genotypes (Fig. 4D). This suggests that the *fer-4* and
246 CRISPR *ralf7x* resistance phenotype is likely independent of altered SA signalling.

247 Jasmonic acid (JA), in concert with ethylene, is usually implicated in defence against insect herbivory
248 and necrotrophic fungi (Bürger and Chory, 2019), but JA treatment can also inhibit colonization by the
249 powdery mildew fungus *Erysiphe cichoracearum* in Arabidopsis (Zimmerli et al., 2004). Importantly, FER
250 inhibits JA signalling by phosphorylating and destabilizing the central JA-associated transcription factor
251 MYC2 (Guo et al., 2018). To test whether FER`s susceptibility role is linked to MYC2-mediated JA
252 regulation, we generated a *fer-4 myc2* mutant via CRISPR-Cas9 in the *fer-4* background that fully
253 diminished MYC2 expression (Fig. S3B, C). Similar to previous reports, mutating *myc2* in *fer-4* partially
254 restored the *fer-4* growth phenotype (Fig. S3D) (Guo et al., 2018). Furthermore, the *fer*-4 CRISPR *myc2*
255 mutant partially complemented the deregulation of JA-responsive genes in *fer*-4, a phenotype that was
256 also observed in CRISPR *ralf7x* and *lrx5x* (Fig. 4E, F, Fig. S3C). Importantly though, mutating *MYC2*
257 did not restore powdery mildew susceptibility in *fer-4* (Fig. 4G, Fig. S3E). This suggests that the
258 resistance phenotype of *fer-4* is independent of MYC2-mediated JA signalling.

259 **Apoplastic pH modulations affect powdery mildew infection success**

260 RALF peptides were first described as potent inducers of apoplastic alkalinisation (Pearce et al., 2010).
261 Similarly, powdery mildew infection of susceptible barley results in transient pH spiking with initial peaks
262 towards the alkaline (Felle et al., 2004). Infiltration of acidic buffers into barley leaves before inoculation
263 with *Blumeria hordei* increases the incidence of papilla formation, indicative of enhanced resistance
264 (Wiese et al., 2004). Since other fungal pathogens also modify the apoplastic pH environment for
265 successful infection (Kesten et al., 2019), we hypothesized that FER-RALF-induced pH modulations
266 affect powdery mildew infection success.

267 Perception of RALF by FER induces the phosphorylation of an inhibitory site on the major Arabidopsis
268 plasma membrane H^+ ATPase AHA1 (Haruta et al., 2014), resulting in its inhibition and apoplastic
269 alkalinisation. AHA1 is the strongest expressed AHA in leaf tissue (Haruta et al., 2010), but the FER-
270 dependent phosphorylation site is conserved in AHA1 and AHA2, the two major isoforms in Arabidopsis.
271 An *aha1* single mutant did not display colonization difference upon *Ecr* infection (Weis et al., 2013).
272 While this might be explained by genetic redundancy, *aha1 aha2* double mutants are seedling lethal,
273 making genetic analysis difficult (Haruta et al., 2010).

274 To determine potential protein interaction partners of FER, we performed a co-immunoprecipiation
275 experiment coupled with a mass spectrometric readout (CoIP-MS). For that we genetically tagged FER

276 with GFP and used a fusion of Lti6b-GFP as negative control, representing a membrane-anchored
277 protein. In this experiment, we could identify 68 potential protein interaction partners of FER, including
278 AHA1 and AHA3 (Fig. S4A, B). Compared to the Lti6b-GFP control sample, the mass spectrometric
279 intensity of AHA1 was 2,7-fold enriched (Fig. 5A), confirming previously published data on AHA1-FER
280 interaction (Du et al., 2016; Haruta et al., 2014). We also found AHA3 to be significantly enriched, since
281 AHA3 derived peptides were only detected in FER-GFP but not in Lti6b-GFP samples. AHA2 was found
282 to be 2,3 -fold enriched (Fig. 5A), but below the significance threshold (FDR<0.05).

283 The majority of the detected protein interaction partners of FER were either RLKs or proteins involved
284 in transmembrane transport (Fig. S4A, B). In particular, we identified four CrRLK1L members (HERK1,
285 MDS1/LET2, THE1 and LET1). We also detected peptides corresponding to the GPI-anchored protein
286 SHAVEN 3 (SHV3) and the closely related SHAVEN3-LIKE1 *(SVL1)*. Double mutants of *SHV3* and
287 *SVL1* (*shv3 svl1*) phenocopy *fer* for increased apoplastic pH, reduced hypocotyl elongation dependent
288 on external sucrose supply, increased cellular sucrose uptake and sucrose-dependent alterations in cell
289 wall contents (Yeats et al., 2016). In response to *Ecr* infection, we could only detect six differential FER-
290 GFP interactors, which may be related to the early experimental time point chosen (1 dpi).

291 Phosphorylation of the C-terminal penultimate threonine residue in AHA1/AHA2 ($AHA1^{T947}/AHA2^{T948}$)
292 activates AHA proton pump activity (Falhof et al., 2016). For example, auxin promotes
293 $AHA1^{T947}/AHA2^{T948}$ phosphorylation in a TRANSMEMBRANE KINASE 1-dependent manner (Lin et al.,
294 2021). We tested whether *Ecr* infection affects $AHA1^{T947}/AHA2^{T948}$ by making use of a phosphosite-
295 specific antibody. However, pT947/pT948 phosphorylation was not altered upon *Ecr* infection, neither
296 in Col-0 nor *in fer-4* (Fig. S6A, B). RALF perception by FER, including RALF1 and RALF23, promotes
297 phosphorylation of serine 899 (pS899) to inhibit AHA1/AHA2 proton pump activity (Haruta et al., 2014;
298 Liu et al., 2025). Importantly, pS899 does not correlate with reduced pT947/pT948 and a recent report
299 showed that RALF23/RALF33 treatment does not induce pT947/pT948 (Haruta et al., 2014; Liu et al.,
300 2025). Therefore, the results do not exclude a FER-dependent regulation of AHA activity and/or proton
301 flux across the plasma membrane correlated with altered *Ecr* infection success. Therefore, we decided
302 to test the *ost2-2D* mutant, which produces a constitutive active AHA1 (Merlot et al., 2007), for altered
303 powdery mildew susceptibility. The *ost2-2D* mutant displayed enhanced *Ecr* resistance (Fig. 5B). The
304 fungal toxin fusicoccin stabilizes 14-3-3 protein interaction with phosphorylation-activated AHA1/AHA2
305 to induce constitutive proton extrusion and can support powdery mildew resistance of barley
306 (Baunsgaard et al., 1998; Zhou et al., 2000). Treatment of plants with fusicoccin before *Ecr* inoculation
307 induced resistance in a partially FER-dependent manner (Fig. 5C, D). Next, we tested whether buffering
308 the apoplastic pH can create an environment that is favourable for the fungus. We hypothesized that
309 alkaline pH infiltration may promote susceptibility and/or break the *fer-4* resistance phenotype, whereas
310 acidic buffers may promote resistance. We infiltrated MES buffer at pH 5,8 (resembling the apoplastic
311 pH) and pH 7,5 into the leaf apoplast prior to infection. Infiltration of a 15 mM $MgCl_2$ solution served as
312 an osmolarity control to exclude effects of high salt concentrations. Surprisingly, both infiltration of the
313 acidic and the alkaline buffers reduced conidiophore production in comparison to the $MgCl_2$ control (Fig.
314 5E). This indicates that *Ecr* requires dynamic pH modulations rather than a fixed (e.g. alkaline) pH for
315 successful host colonization. When analysing individual fungal colonies upon infection on Col-0 pre-

316 buffered leaves we observed a morphological similarity between fungal colonies on *fer-4* with normal
317 hyphal growth but strongly reduced conidiophore production at 5 dpi (Fig. 5F). This observation suggests
318 the importance of apoplastic pH modulations for successful conidiophore production of *Ecr* at later time
319 points of the infection, which may be regulated through FER-RALF-dependent signalling.

320 Among other physiological outputs, apoplastic pH modulation is involved in plant growth regulation by
321 controlling the activity of PECTIN METHYL ESTERASES (PMEs) (Hocq et al., 2023; Hocq et al., 2016;
322 Sénéchal et al., 2017). PMEs de-esterify cell wall pectins, which increases the negative charge of
323 homogalacturonans resulting in enhanced Ca^{2+} binding and pectin cross-linking which stiffens the cell
324 wall (Willats et al., 2001). Importantly, demethylated pectin interacts with LRX-RALF complexes to
325 structurally organize the cell wall of root hairs and pollen tubes to support polar growth (Moussu et al.,
326 2023; Schoenaers et al., 2024). PMEs are also involved in biotic interactions. For example, *AtPME17*
327 expression is strongly up-regulated during infection with the necrotrophic fungus *Botrytis cinerea* and
328 *pme17* mutants are more susceptible to infection (Del Corpo et al., 2020). Recently, *fer-4* mutants were
329 shown to have constitutively increased PME activity (Biermann et al., 2024). In accordance with LRX
330 and RALF-peptides being involved in the same physiological pathway as FER, PME activity was
331 similarly enhanced in *lrx5x* and CRISPR *ralf7x*. *Ecr* infection, however, had no effect on PME activity in
332 the harvested leaf samples at 5 dpi (Fig. 5G). To test whether PME-mediated pectin demethylation
333 affects powdery mildew infection, we infiltrated single leaves with epigallocatechin gallate (EGCG), a
334 compound from green tea (Camellia sinensis) that inhibits PMEs (Lewis et al., 2008). qPCR analysis
335 of the infiltrated leaves at 5 dpi revealed reduced fungal DNA content on Col-0 leaves infiltrated with
336 EGCG, indicating that PME activity is potentially required for successful powdery mildew colonization.
337 Interestingly, EGCG treatment had no additive effect on the resistance of *fer*-4 mutants (Fig. 5H). To
338 complement the inhibitor treatment experiment, we tested the effect of PME-inhibitor (PMEI)
339 overexpression on *Ecr* colonization. PMEIs inhibit PMEs *in vivo* in a pH dependent manner to fine-tune
340 cell wall remodelling. Overexpression of *PMEI3* was recently shown do inhibit RALF1 signalling in roots
341 (Rößling et al., 2024). In line with the EGCG treatment, inhibition of PME activity by *PMEI3*
342 overexpression resulted in reduced fungal colonization (Fig. 5I). Knockout of single *PMEs,* however,
343 had not effect on conidiophore production, most likely due to high redundancy of PMEs in Arabidopsis
344 (Fig. 5J). Taken together, we could show that PME activity, which also affects FER-dependent RALF
345 signalling, is required for full powdery mildew susceptibility.

346 **RALF-mediated powdery mildew susceptibility is partially independent of FER and FER-**
347 **signalling**

348 The reduced *Ecr* infection success upon pH buffering prompted us to resolve potential infection-induced
349 apoplastic pH changes with cellular resolution. For this we used the ratio-metric pH sensor
350 pUBQ10::SYP122-pHusion (Kesten et al., 2019). We detected an increase in the apoplastic pH close to
351 *Ecr* penetration sites at 2 dpi. Surprisingly, similar infection-related pH increase was observed in a
352 CRISPR-Cas9-generated *fer* mutant (CRISPR *fer*) in the pUBQ10::SYP122-pHusion line (Fig. 6A, B).

353 When mining the CoIP-MS data for changes in protein phosphorylation upon *Ecr* infection we found the
354 tendency to enhanced phosphorylation in two areas of the FER intracellular kinase domain, including

355 the area around amino acid position 511-518 as well as 861-874 (Fig. S7A). The phosphorylation sites
356 pS500 and pS881, on the other hand, were not regulated (Fig. S7A). The site pS874 has been previously
357 reported to be phosphorylated upon RALF1 treatment (Haruta et al., 2014). This provides indications
358 that FER undergoes *Ecr*-dependent phosphorylation, which prompted us to test whether FER kinase
359 activity is required for *Ecr* colonization. Experiments using a kinase dead FER variant (FER^{K565R})
360 complemented the powdery mildew resistance phenotype of *fer-4*, suggesting that FER kinase activity
361 is dispensable for powdery mildew susceptibility (Fig. 6C).

362 To assess whether FER recruitment to RALF-LLG1 complexes is required for *Ecr* susceptibility, we
363 infected *fer-4* lines expressing structure-guided FER mutants disrupting the LLG binding interface (Xiao
364 et al., 2019). Both FER^{N303Y} and FER^{G257A} fully restored powdery mildew susceptibility, indicating that
365 RALF-induced recruitment of FER to LLG1 is not essential for powdery mildew infection (Fig. 6D). We
366 thus asked the question whether the susceptibility function of RALFs is primarily attributed to structural
367 functions rather than FER-LLG-dependent signalling. Therefore, we introduced structure-guided
368 mutations into RALF23, either disrupting the predicted LRX-binding interface ($RALF23^{Y113A/Y114A}$),
369 analogous to $RALF4^{Y83A/Y84A}$ (Moussu et al., 2020) or the YISY motif required for LLG binding and FER-
370 dependent signalling ($RALF23^{Y93A/Y96A}$) (Xiao et al., 2019) and expressed both variants under control of
371 the 35S promoter in CRISPR *ralf7x*. We tested two lines each with CRISPR *ralf7x* p35S::$RALF23^{Y93A/Y96A}$
372 displaying similar expression levels as the WT complementation lines. CRISPR *ralf7x*
373 35S::$RALF23^{Y113A/Y114A}$ lines showed weaker expression compared to the WT construct (Fig. S2E, F).
374 The weaker expressing $RALF23^{Y113A/Y114A}$ lines could not complement the CRISPR *ralf7x* growth and
375 enhanced *Ecr* resistance phenotype (Fig. 6E, Fig. S8A). RALF23 $^{Y93A/Y96A}$ largely complemented the
376 growth phenotype (Fig. S8A). However, $RALF23^{Y93A/Y96A}$ showed moderate but incomplete
377 complementation in powdery mildew infection (Fig. 6E). Together, this data suggests that both
378 interaction of RALF23 with LLG and LRX complexes is required to support *Ecr* colonization.

379 We next tested whether application of synthetic RALF23 peptide can affect powdery mildew infection
380 success in a FER-dependent manner. In plant-bacterial interaction, co-treatment with RALF23 reduced
381 PAMP-triggered resistance to *Pto* infection (Stegmann et al., 2017). Surprisingly, RALF23 infiltration into
382 single leaves 24 h prior to *Ecr* infection had a mild resistance-inducing effect in Col-0 (Fig. 6F). This
383 indicates that infiltration of high doses of a peptide at a fixed time point induces antagonistic responses,
384 in line with a recent report showing differential concentration-dependent effects of RALF23 on root
385 immunity (Chen et al., 2024). Remarkably, RALF23 infiltration increased conidiophore production in the
386 *fer-4* mutant background, suggesting that RALF23 exerts FER-independent effects (Fig. 6F). Based on
387 this we continued testing the effect of RALF23-GFP overexpression on *Ecr* infection outcome,
388 comparing Col-0 with the *fer-2* mutant. RALF23-GFP overexpression suppresses PAMP-triggered
389 responses in a FER-dependent manner (Stegmann et al., 2017). Similar to exogenous RALF23 peptide
390 treatment (Fig. 6F), RALF23-GFP overexpression mildly promoted resistance to *Ecr*. Strikingly,
391 RALF23-GFP overexpression restored susceptibility in the *fer-2* mutant background (Fig. 6G). *RALF23-*
392 *GFP* showed similar transcript abundance in Col-0 and *fer-2* (Fig. S7B). Collectively, based on these
393 data we hypothesize that RALF-mediated powdery mildew susceptibility is at least partially FER-
394 independent.

395 **Discussion**

396 This work provides first molecular insights into the mechanism of FER-mediated powdery mildew
397 susceptibility. We revealed that FER`s RALF peptide ligands are critical for the completion of *Ecr*`s
398 asexual life cycle upon host colonisation.

399 RALFs are perceived by LLG-FER/CrRLK1L complexes to induce downstream signalling. The kinase
400 domain of FER displayed a tendency towards increased phosphorylation of several residues upon *Ecr*
401 infection, but a kinase dead FERK^{565R} fully complemented the *Ecr* colonization phenotype of *fer-4.* FER
402 kinase activity is not required for all FER-related outputs. The *fer-4* defects in ovule fertilization and
403 FLS2-BAK1 complex formation are fully complemented by FER kinase dead variants (Gronnier et al.,
404 2022; Haruta et al., 2018). RALF1-induced calcium influx and root growth inhibition is dependent on
405 FER kinase activity, but *fer-4* FERK^{565R} lines retain mild RALF1 sensitivity (Haruta et al., 2018).
406 Moreover, FER^{K565R} confers sensitivity to RALF1-induced stomatal closure in a protein accumulation-
407 dependent manner, suggesting that FER kinase activity is required for RALF signalling, but can be
408 compensated by higher protein doses (Chakravorty et al., 2018). Disrupting FER`s LLG1 binding
409 interface was also dispensable for *Ecr* colonization. Yet, RALF binding to LLG1 contributes to
410 susceptibility, since *llg1-3* mutants with disrupted RALF binding were more resistant to *Ecr* colonization
411 and, importantly, RALF23 mutants with compromised YISY motif required for LLG binding and CrRLK1L-
412 dependent signalling (Xiao et al., 2019) failed to fully complement the *Ecr* resistance phenotype of
413 CRISPR *ralf7x*. This suggests that RALF-mediated *Ecr* susceptibility is associated with RALF-induced
414 signalling but not strictly dependent on FER and/or FER kinase activity. Consistently, the CRISPR *ralf7x*
415 mutant was more resistant than *fer-4,* and *fer* loss of function mutants displayed increased *Ecr*
416 susceptibility upon RALF23 treatment or RALF23-GFP overexpression, reinforcing at least partially
417 FER-independent functions of RALF-peptides during *Ecr* colonization. FER is dispensable for RALF22-
418 induced root hair tip alkalinisation, calcium influx and cell wall modification (Schoenaers et al., 2024)
419 and RALF23 affects cell wall pectin status in a partially FER-independent manner (Biermann et al.,
420 2024), further supporting FER-independent functions of RALF peptides in vegetative physiological
421 outputs. Our data raises the question whether additional FER-related receptors are required to establish
422 full susceptibility. We speculate that LLGs may recruit further FER-related CrRLK1L proteins that
423 redundantly support host mildew colonization.

424 FER can interact with related RALF-binding CrRLK1Ls, including HERK1 and ANJ, to form higher order
425 complexes. This was confirmed by our CoIP-MS data according to which FER interacted with several
426 members of the CrRLK1L family (HERK1, MDS1, THE1 and LET1) in mature leaves. HERK1 associates
427 with FER on papilla and synergid cells to control RALF-induced pollen tube penetration (Galindo-Trigo
428 et al., 2020; Lan et al., 2023). MDS1 (also known as LET2) and LET1 have a role in SUMM2-mediated
429 cell death regulation (Huang et al., 2020; Liu et al., 2020). A LET1/LET2 function in RALF perception
430 remains unknown, but LET2 and LET1 form heteromers and associate with LLG1, suggesting
431 participation in higher order CrRLK1L-RALF complexes (Huang et al., 2020). THE1 perceives RALF34
432 (mutated in CRISPR *ralf7x*) and RALF34's seedling growth inhibition and alkalinisation activity does not
433 require FER (Abarca et al., 2021). Our CoIP-MS data revealed also other FER-associated RLKs, in line
434 with the proposed role of FER as a RLK scaffold (Stegmann et al., 2017). Future work should analyse

435 combinatorial CrRLK1L mutants for increased *Ecr* resistance and subsequent biochemical analysis for
436 *Ecr*-dependent CrRLK1L association and phosphorylation.

437 RALF binding to LRXs shapes the organization of the cell wall in root hair cells and growing pollen tubes
438 (Moussu et al., 2023; Schoenaers et al., 2024). We identified LRX1-LRX5 as powdery mildew
439 susceptibility factors, suggesting that the structural role of LRX-RALF complexes contributes to fungal
440 host establishment. Consistently, a RALF23 LRX binding interface mutant failed to complement the
441 CRISPR *ralf7x Ecr* phenotype and overexpression of LRR4-citrine, which lacks the LRX4 extensin
442 domain, conferred enhanced powdery mildew resistance. LRR4-citrine imposes a dominant negative
443 phenotype in several LRX-related vegetative physiological outputs (Dünser et al., 2019; Zhao et al.,
444 2018), likely by sequestration of RALFs, outcompeting of endogenous LRXs and interference with their
445 cell wall organizing properties. However, LRX1/LRX2 are also required for RALF22 secretion
446 (Schoenaers et al., 2024). We hence cannot exclude that the *lrx5x Ecr* phenotype is explained by the
447 lack of signalling competent RALF accumulation in the apoplast. RALFs bind to LRX with high affinity at
448 acidic pH, while LLG2 requires alkaline conditions for optimal RALF recognition (Moussu et al., 2020),
449 indicating that pH-dependent coordinated binding and release of RALFs by LRXs could be involved in
450 CrRLK1L-dependent signalling. It is thus possible that dynamic apoplastic alkalinisation induced by *Ecr*
451 infection releases RALFs from LRXs to trigger CrRLK1L-dependent signalling events that further support
452 its reproductive success.

453 Our work also revealed first downstream mechanistic insights into RALF-FER/LLG1 and/or RALF-LRX-
454 dependent pathways required for successful *Ecr*-Arabidopsis interaction. The powdery mildew
455 resistance phenotype of *fer-4* was not attributed to de-regulated SA or JA signalling, suggesting a
456 different type of underlying mechanism. Our genetic and cell biological data indicate that FER and RALF-
457 mediated powdery mildew colonization is not directly linked to *MLO*-mediated penetration success. Our
458 data rather supports that FER-RALF is required for maintenance of compatibility and post-penetration
459 completion of *Ecr*`s asexual life cycle. The *mlo6* single mutants do not show defects in *Golovinomyces*
460 *orontii* epidermal cell penetration, but a trend towards reduced conidiophore production. The *mlo2* single
461 mutant still maintains ~50% of host cell entry, but abolished conidiophore production (Consonni et al.,
462 2006), raising the question whether MLO also contributes to long-term host association. Therefore, our
463 data does not exclude a role of RALF-induced and MLO-dependent signalling required for *Ecr*
464 sporulation. We also cannot fully rule out that FER and/or RALFs may act redundantly with other
465 CrRLK1Ls/RALFs to contribute to *Ecr* epidermal cell penetration.

466 Our data suggests that powdery mildew susceptibility requires functional apoplastic pH homeostasis
467 and modifications of the cell wall pectin methyl-esterification status, both processes in which FER-RALF
468 and/or LRX-RALF modules fulfil central regulatory functions. Constitutive AHA1 activity in *ost2-2D*
469 mutants or fusicoccin treatment promoted powdery mildew resistance. Importantly, fusicoccin treatment
470 was less effective in *fer-4*, suggesting that mutating FER and chemically activating AHA1 affects the
471 same pathway. It is also possible that fusicoccin treatment cannot further promote apoplastic
472 acidification in *fer-4*, which displays constitutively elevated proton extrusion. Earlier work revealed that
473 barley powdery mildew infection is accompanied by pH shifts and the induction of apoplastic
474 alkalinisation (Felle et al., 2004). Importantly though, mildew-induced pH shifts were dynamic, with

475 fluctuations between alkaline and more acidic conditions (Felle et al., 2004). This supports our notion
476 that disrupting apoplastic pH homeostasis by buffering inhibits *Ecr* host colonization.

477 Our data further reveals that the pectin methylation status determines powdery mildew pathogenesis.
478 Overexpression of PMEI3 and EGCG treatment, a well-established chemical PME inhibitor, promoted
479 *Ecr* resistance. PMEI3 inhibits PME3, which is involved in FER-mediated epidermal cell lobing (Lin et
480 al., 2022). We could not resolve *Ecr* phenotypes in *pme3* loss of function mutants, suggesting
481 redundancy with other PMEs in this 66 member multi-gene family in Arabidopsis (Harholt et al., 2010;
482 Pelloux et al., 2007). PMEI3 activity is strongly pH dependent with the highest activity at acidic conditions
483 (Xu et al., 2022). RALF-induced apoplastic alkalinisation may inhibit PMEI3, promoting PME activity for
484 cell wall remodelling. RALF22, and RALF4 bind to LRXs to regulate pectin compaction in the cell wall.
485 LRXs shape RALFs to expose a polycationic region for interaction with de-methylated and acidic pectin
486 (Moussu et al., 2023; Schoenaers et al., 2024). Moreover, PME activity is required for RALF1-induced
487 root growth inhibition independent of LRX1-LRX5 (Rößling et al., 2024) and RALF1 forms molecular
488 condensates with pectin required for downstream FER-LLG1-dependent responses (Liu et al., 2024).
489 Strikingly, a RALF1 mutant that is compromised in binding to FER-LLG1 and does not induce
490 alkalinisation (Liu et al., 2024; Pelloux et al., 2007; Stegmann et al., 2017) fails to form RALF-pectin
491 condensates (Liu et al., 2024), suggesting that RALF-pectin association and signalling outputs are
492 intimately interconnected. Our work revealed that *fer*, CRISPR *ralf7x* and *lrx5x* display elevated steady-
493 state PME activity, an output that was unaffected by *Ecr* infection and is in accordance with previous
494 findings (Biermann et al., 2024). This may be explained by the requirement of de-methylated pectin for
495 RALF signalling and that the absence of LRX-RALFs and CrRLK1L-LLG-RALFs might activate plant
496 feedback mechanisms to promote PME activity. Pectin de-methylation is an irreversible process. The
497 high steady-state PME activity in *fer-4* may thus explain the reduced effect of EGCG-promoted *Ecr*
498 resistance. The *fer-4* mutant may accumulate high levels of de-methylated pectin in the cell wall,
499 abrogating a detectable effect by apoplastic PME inhibition. FER is required for expression of the
500 polygalacturonase ADPG1 upon disruption of lignin biosynthesis (Liu et al., 2023), reinforcing the
501 function of FER-dependent cell wall remodelling during stress. We propose a mechanism in which pH-
502 dependent pectin de-methylesterification is a prerequisite for RALF-mediated sustained powdery mildew
503 host colonization. In accordance, endogenous pectin modification affects powdery mildew infection
504 outcome. Mutants in the pectate *lyase POWDERY MILDEW RESISTANT 6 (PMR6)* are more resistant
505 to *Golonivomyces cichoracearum* with normal host penetration, delayed fungal spread, strongly reduced
506 sporulation and normal SA/JA signalling (Vogel et al., 2002), resembling phenotypes of CRISPR *ralf7x*
507 and *fer-4*. PME-induced pectin demethylation is a prerequisite for pectate lyase-mediated degradation
508 (Wormit and Usadel, 2018). Yet, PME inhibition, which should reduce PMR6 activity, and PMEI over
509 accumulation, which should promote pectate lyase activity, limit fungal colonization, reinforcing the
510 notion that fine-tuned pectin remodelling, in concert with dynamic apoplastic pH modulations, underlies
511 powdery mildew reproductive success.

512 *Ecr* conidiation likely requires significant energy input and it remains unclear how disruption of the RALF
513 pathway and/or pH and cell wall dynamics affects this process. The fungal haustorium is surrounded by
514 the extrahaustorial matrix (EHMx) and the extrahaustorial membrane (EHM), a plant membrane that is

515 continuous with the plasma membrane but has distinctive properties (Hückelhoven and Panstruga,
516 2011; Polonio et al., 2021). At the site of invasion the extrahaustorial matrix is sealed with densely
517 packed cell wall depositions forming the haustorial neck region (Micali et al., 2011). This renders the
518 EHMx a separate apoplastic compartment that can have different conditions compared to the
519 neighbouring plant cell wall (Hückelhoven and Panstruga, 2011). Nutrient uptake from the EHMx is most
520 likely dependent on the compartments pH. From rust fungi it is known that ATPase activity is enhanced
521 in haustorium derived membrane vesicles compared to other fungal structures, indicating a role of fungal
522 ATPases in nutrient uptake via H^+ symporters (Voegele and Mendgen, 2011). The nutrients that are
523 found in the EHMx and taken up by the fungus should derive from the invaded plant cell. They must first
524 be exported from the host cell before they are available to the fungus. Nutrient export from the plant cell
525 involves SWEET proteins and the uptake is facilitated by sucrose transport proteins (STP), both of which
526 control apoplastic sugar levels and affect plant microbe interactions (Bezrutczyk et al., 2018). STPs
527 usually transport sugars from the apoplast into the plant cell and control available sugars for microbial
528 invaders (Geiger, 2020). In Arabidopsis, AtSTP8 localizes to the EHM and overexpression of AtSTP8
529 increases susceptibility to powdery mildew, indicating that STP8 is involved in nutrient supply (Liu et al.,
530 2021). *STP4* expression in leaves is enhanced after powdery mildew infection (Fotopoulos et al., 2003)
531 and STP13 is associated with resistance to both powdery mildew and rust fungi in wheat and barley
532 (Milne et al., 2019). Perception of flg22 by FLS2-BAK1 results in STP13 phosphorylation to enhance
533 cellular uptake capacity and limit apoplastic sugar availability for bacterial pathogens (Yamada et al.,
534 2016). STPs are H^+ symporters, and STP8 has a pH optimum at 5,5 for cellular import (Liu et al., 2021).
535 Disruption of pH dynamics through mutating RALF-CrRLK1L could impair nutrient supply by affecting
536 spatiotemporal export of nutrients to the EHMx and interfering with fungal uptake. In accordance, *fer*
537 mutants show enhanced sucrose uptake, starch accumulation and hypersensitivity to exogenous
538 sucrose treatment, a phenotype shared with *shv3 svl1* mutants (Yang et al., 2015; Yeats et al., 2016).
539 The *shv3 svl1* mutants also display reduced apoplastic pH (Yeats et al., 2016) and we identified SHV3
540 as an FER interactor. Since RALF1`s effects on pH-dependent root growth likely do not involve direct
541 FER-mediated AHA regulation, FER may also induce cellular H^+ import to counteract apoplastic
542 acidification via yet unknown transporters (Li et al., 2022a). It is possible that *Ecr* infection induces
543 RALF-CrRLK1L-dependent changes to the apoplastic pH that will reprogram transporter topology to
544 favour haustorial sugar uptake over plant cell import. Supporting our hypothesis, we identified several
545 proteins associated with transmembrane transporter activity as FER interactors in our Co-IP MS
546 experiment. This includes STP1, involved in resistance against bacterial infection, the ABC transporter
547 PEN3, associated with Arabidopsis host and non-host resistance against powdery mildew, and the
548 PLASMA MEMBRANE INTRINSIC 2;2 (PIP2;2) aquaporin, a recently discovered FER target (Collins et
549 al., 2003; Liu et al., 2025; Stein et al., 2006; Yamada et al., 2016). We propose that FER`s interaction
550 with membrane localized transport proteins and the pH-regulatory function of RALF-CrRLK1L modules
551 shape the transporter landscape at the host-*Ecr* interface to support colonization. Moreover, RALFs may
552 control the pectin methylesterification status of the cell wall surrounding powdery mildew penetration
553 sites. Methylated or demethylated pectins have not been detected at the haustorial neck region, which
554 does not exclude a role for fungal accommodation in the neighbouring cell wall (Micali et al., 2011).
555 Moreover, *fer* mutants show reduced cell wall cellulose content, further suggesting structural defects

556 that may impact *Ecr* host interaction. We speculate that this could control the ability of the fungus to
557 establish a defined pH environment for optimising transporter-mediated nutrient uptake. Future studies
558 should dissect the plant-*Ecr* interface in *FER/LRX-RALF*, pH and cell-wall related mutants with
559 ultrastructural analysis by electron microscopy.

560 Other plant pathogens produce RALFs to establish host colonization, including *Fusarium oxysporum*
561 and root knot nematodes (Masachis et al., 2016; Zhang et al., 2020). Interestingly, these RALF peptide
562 mimics lack conserved sequence elements required for LRX binding, but contain a modified YISY motif
563 required for LLG-CrRLK1L-dependent signalling (Pearce et al., 2010). This suggests that fungal RALFs
564 solely rely on CrRLK1L-induced signalling outputs and not on structurally re-shaping cell wall
565 architecture for their virulence function. None of the analyzed powdery mildew genomes contained RALF
566 peptide mimics, suggesting that *Ecr* likely relies on the combination of endogenous RALF signalling and
567 cell wall remodelling to support sustained host interaction. Our work thus highlights a novel mode of
568 RALF function, combining signalling and structural roles for the control of plant microbe interactions.

569

570 **Materials and Methods**

571 **Powdery mildew propagation**

572 Powdery mildew fungi of the species *Erysiphe cruciferarum* were propagated weekly by transferring
573 spores to 4 – 5 week old uninfected Col-0 plants. Powdery mildew spores were used for further
574 inoculation 3 – 4 weeks after propagation. Powdery mildew propagation and infection experiments were
575 performed in an environmentally controlled growth cabined (22 °C, 70 % relative humidity, 12 h
576 photoperiod).

577 **Molecular cloning**

578 To generate p35S::RALF23 and p35::MLO2-mCherry lines the respective gene sequences were cloned
579 from gDNA using the primers listed in Table S3 and assembled into a GoldenGate-modified pCB302
580 binary vector for plant expression. The structure guided RALF23 mutant lines p35S::RALF23$^{Y93A/Y96A}$
581 and p35S::RALF23$^{Y113A/Y114A}$ were obtained by site-directed mutagenesis using the respective primers
582 listed in Table S3 and likewise assembled into a GoldenGate-modified pCB302 binary vector for plant
583 expression. To generate CRISPR-Cas9 mutants the software tool chopchop
584 (https://chopchop.cbu.uib.no/) was used to design target sites in the respective genes (1 to 2 per gene
585 of interest). All target sequences used in this study are listed in Table S4. Individual guide RNAs with
586 gene specific target sites were obtained by gene synthesis (Twist Bioscience, USA). Using a
587 GoldenGate-adapted pUC18-based vector the guide RNA fragments were assembled. Higher order
588 gRNA stacks were cloned into pICSL4723OD with FastRed-pRPS5::Cas9 (Castel et al., 2019). For final
589 floral dip transformation of Arabidopsis all generated plant expression constructs were transformed into
590 *Agrobacterium tumefaciens* strain GV3101.

591 **Plant material and growth conditions**

592 Plant lines used in this study are listed in Table S2 with the according references.
593 Isolation of homozygous CRISPR mutants was done based on red fluorescence of transformed seeds.
594 In the T1 generation red fluorescent seeds were selected and grown on soil for genotyping with gene
595 specific primers. In the T2 generation mutants lacking the transgene were identified based on the loss
596 of fluorescence. Simliarly, homozygous p35S::MLO2-mCherry lines were selected based on red
597 fluorescence. Homozygous p35S::RALF23 lines were selected by transgene mediated BASTA
598 resistance. All plants were vernalized for 2 – 3 days in the dark at 4 °C and grown with two plants per
599 pot in environmentally controlled conditions (21 °C, 55 – 65% relative humidity, 8 h photoperiod). Five
600 to six week-old plants were used for infection.

601 **Conidiophore counting and fungal penetration assay.**

602 Conidiophore production was analysed 5 days after infection with *Ecr*. Four leaves per genotype were
603 harvested from 4 individual infected plants. The leaves were destained using EtOH:Acetic Acid (6:1)
604 and subsequently stained using ink (ink: 25 % acetic acid, 9:1). Ink-stained fungal structures were
605 visualized using the Zeiss AXIO imager Z1.m microscope with a 20x magnification for conidiophore
606 counting. Fungal penetration success was similarly analysed and quantified at 2 dpi. A penetration
607 attempt was scored as successful when the spore formed a penetration tube and first hyphal structures.
608 The host cell entry rate was determined by the number of successful penetrations per attempts (in %).

609 **Quantification of fungal DNA by qPCR**

610 For quantification of fungal DNA two infected plants per genotype were harvested at 5 dpi. Plant material
611 was ground in liquid nitrogen and equal amounts of plant powder was transferred into a 2 ml Eppendorf
612 tube. 500 µL extraction buffer (200 mM Tris-HCl pH 7,5, 250 mM NaCl, 25 mM EDTA, 0,5 % SDS) were
613 added per sample. After vortexing, 500 µL chloroform was added with subsequent mixing. After
614 centrifugation, the top layer was transferred into 500 µL isopropanol and mixed. The DNA pellet was
615 precipitated by centrifugation and washed with 70 % EtOH before resuspension in 50 µL water and
616 measurement of DNA concentration. For qPCR, the DNA concentration was adjusted to 20 ng/µL for all
617 samples. RT-qPCR experiments were performed using Maxima SYBR green mix (Thermo Fisher
618 Scientific, USA) on an AriaMx Real-Time PCR system (Agilent Technologies, USA). The amount of
619 fungal DNA was calculated relative to the amount of plant DNA using primers for the Arabidopsis small
620 RubisCO subunit (AtRbcS) and *Ecr* tubulin (Table S3). All samples were normalized to Col-0.

621 **Infiltration experiments**

622 For RALF peptide treatment individual leaves were infiltrated with 1 µM synthetic RALF23 peptide
623 (Sequence: ATRRYISYGALRRNTIPCSRRGASYYNCRRGAQANPYSRGCSAITRCRRS) 24 h prior to
624 infection. Fusicoccin (10 µM) and EGCG (50 µM) and MES buffers were infiltrated 2 h before *Ecr*
625 infection and subsequent microscopical analysis or qPCR-mediated assessment of infection success at
626 5 dpi.

627 **Gene expression analysis**

628 Expression of SA and JA responsive genes was analysed at 5 dpi upon *Ecr* infection. Four individual
629 plants were harvested per genotype and immediately frozen in liquid nitrogen. The plant material was

630 ground and equal amounts of plant powder were transferred into individual 2 ml Eppendorf tubes. For
631 RNA extraction, TRIzol reagent (Roche, Switzerland) and subsequent purification with Direct-zol™ RNA
632 Miniprep Plus kit (Zymo Research, Germany) with on column DNAse I digestion was used. 1.5 – 2 µg
633 of total RNA was reverse transcribed with random hexamer primer and Revert Aid reverse transcriptase
634 (Thermo Fisher Scientific, USA). RT-qPCR experiments were performed using Maxima SYBR green
635 mix (Thermo Fisher Scientific, USA) on an AriaMx Real-Time PCR system (Agilent Technologies, USA).
636 Expression levels of the tested genes were normalized to the house-keeping gene *UBIQUITIN 5*
637 (*UBQ5*). All primers used for gene expression analysis are listed in Table S3.

638 **PME activity assay**

639 PME activity assays were performed as previously described (Bethke et al., 2014). In brief, plant material
640 of untreated and infected plants was harvested 5 dpi and ground in liquid nitrogen. Equal amounts of
641 plant material were transferred per genotype and treatment into individual 2 ml tube. The plant powder
642 was incubated with 500 µL protein extraction buffer (50 mM Tris-HCl pH 7.5, 150 mM NaCl, 10%
643 glycerol, 5 mM dithiothreitol, 1% protease inhibitor cocktail, 2 mM Na2MoO4, 2.5 mM NaF, 1.5 mM
644 activated Na3VO4, 1mM phenylmethanesulfonyl fluoride, 0.5% IGEPAL) for 30 min at 8°C before
645 centrifugation at 16,000 g for 30 min. The supernatant was transferred into a fresh 1,5 ml tube and the
646 protein concentration was determined by Bradford assay. The protein concentration was adjusted to 3
647 µg/µL. To assess PME activity, the liquid was loaded into holes in an agarose gel plate containing
648 esterified pectin (1.2 % (w/v) agarose, 0.1 % (w/v) pectin from apple, 12 mM citric acid, 50 mM Na_2HPO_4
649 pH 7). Per hole 15 µL liquid were loaded and 4 technical replicates were performed per genotype and
650 treatment. The plates were incubated at 37°C for 16 h. After incubation, plates were briefly washed with
651 water and stained with 0.05 % ruthenium red for 30 min. Residual dye was washed off with water and
652 images of the plates were captured by scanning. Darker stained areas correlating with PME activity
653 were quantified using Fiji ImageJ software.

654 **AHA-phosphorylation analysis**

655 Infected plant material was harvested 3 dpi and ground in liquid nitrogen. 20 µL extraction buffer (3 %
656 [w/v] SDS, 30 mM TRIS-HCl pH 8.0, 10 mM EDTA. 10 mM NaF, 30 % [w/v] Sucrose, 0.012% [w/v]
657 Coomassie Brilliant Blue, 15 % [v/v] 2-Mercaptoethanol) per mg plant material was added and samples
658 were vortexed two times for 30 sec. Subsequently, samples were centrifuged at 12,000 x g for 1 min.
659 The supernatant was immediately used for SDS PAGE and western blot. Protein bands were detected
660 using polyclonal AHA and pThr947 antibodies (Hayashi et al., 2010). Band intensities were quantified
661 using Fiji ImageJ software.

662 **Quantification of salicylic acid, dihydroxybenzoic acids and camalexin**

663 For the quantification of salicylic acid (SA), dihydroxybenzoic acids (DHBAs) and camalexin 40-60 mg
664 of ground fine leaf powder was extracted as described by (Nawrath and Métraux, 1999) with minor
665 modifications. First, 600 µl 70% methanol containing 250 ng of *ortho*-anisic acid (oANI) as internal
666 standard were added and samples were incubated for 1 hour at 65°C. The samples were centrifuged
667 for 1 min at 14,000 x g and the supernatant was collected in a fresh reaction tube. The powder was re-

668 extracted with 600 µl of 90% methanol for 1 hour at 65°C, centrifuged as before and the supernatants
669 were combined. The solvent was evaporated using a rotational vacuum concentrator for 2.5 hours at
670 35°C and 10 mbar. After a precipitation step with 500 µl of 5 % trichloroacetic acid and centrifugation
671 for 10 min at 3,500 x g, the supernatant was transferred in a fresh reaction tube and partitioned against
672 600 µl cyclohexane / ethyl acetate (1:1). The samples were shaken, centrifuged for 10 min at 3,500 x g
673 and the organic (upper) phase was transferred in a fresh reaction tube. The partitioning step was
674 repeated and the organic phases combined to obtain free SA, DHBAs and camalexin. For the extraction
675 of the glycosylated SA and DHBAs, the aqueous phase was acidified by adding 8 M hydrochloric acid
676 (1:1) and incubated for 1 hour at 80°C. Again, 250 ng of oANI were added and the hydrolyzed extracts
677 partitioned two times against 600 µl cyclohexane / ethyl acetate (1:1) as described above to obtain
678 glycosylated SA and DHBAs. All organic phases (free and glycosylated fractions) were evaporated using
679 a rotational vacuum concentrator to near dryness to prevent sublimation of SA. The reduced extracts
680 were dissolved in 400 µl of 90% 25 mM potassium dihydrogen phosphate buffer (KH_2PO_4), pH 2.6, and
681 10% acetonitrile (ACN). HPLC analysis was performed on an Agilent Technologies 1260 Infinity II
682 system equipped with an G7121B fluorescence detector (Agilent Technologies, USA). SA, DHBAs,
683 camalexin and oANI were separated on a SecurityGuard Ultra guard column (3 mm; Phenomenex, USA)
684 followed by an InfinityLab Poroshell 120 SB-C18 analytical column (3 x 100 mm, 2.7 µm; Agilent
685 Technologies, USA) at 40°C. The separation was performed with a solvent gradient of eluent (A) 25mM
686 KH_2PO_4, pH 2.6 and eluent (B) ACN:H_2O (99:1) at 1 ml/min flow rate (all steps in v/v): 0 to 1 min: 10%
687 B; 1 to 6 min: 10 – 25 %B; 6 to 8.5 min: 25 – 80 %B; 8.5 to 10.5 min: 80% B; 10.5 to 11 min: 80 – 10%
688 B; 11 to 14 min 10% B. The fluorescence detector was used to detect oANI (excitation 305 nm, emission
689 365 nm), SA (excitation 305 nm, emission 407 nm), DHBAs (excitation 320 nm, emission 450 nm) and
690 camalexin (excitation 318 nm, emission 370 nm). For quantification, standard dilution series of oANI,
691 SA, 2,3-DHBA, 2,5-DHBA and camalexin were measured in the range of 1 to 100 ng.

692 **Histochemical staining of callose deposition in rosette leaves and trichomes**

693 Three rosette leaves per 35-d-old Arabidopsis plant were collected in 2-mL reaction tubes and destained
694 twice for 24 h each in 70% ethanol (v/v). Afterwards, rosette leaves were incubated over-night in aniline
695 blue solution (0.01% Aniline Blue (m/v) in 150 mM dipotassium hydrogen phosphate buffer) and
696 mounted on a microscopy slide. Micrographs were captured by a BZ-9000 transmitted light and
697 fluorescence microscope (Keyence, Osaka, Japan) using UV illumination. Images were optimized by
698 Adobe Photoshop 2024 in an identical manner for all micrographs. Trichome and trichome branch
699 number were scored by counting.

700 **Confocal microscopy**

701 Confocal laser-scanning microscopy was performed using a Leica TCS SP5 (Leica, Germany)
702 microscope (with Leica Application Suite X 3.7.4.23463). All images were taken with a 20 x water
703 immersion objective. To analyse the localization of FER-GFP and MLO2-mCherry, adult plants were
704 infected with *Ecr* and imaged at 2 dpi. To visualize GFP fluorescence an argon laser with an emitting
705 wavelength of 488 nm was used and the GFP signal was detected from 500 nm to 550 nm with a HyD
706 detector. The mCherry fluorophore was excited with a DPSS 561 laser emitting at 561 nm and a

707 detection window of 600 - 640 nm. Changes in the apoplastic pH around fungal infection sites were
708 analysed using plant lines expressing the pUBQ10::SYP122-pHusion. Four to five week-old plants were
709 infected with *Ecr* and confocal imaging was performed at 2 dpi. The GFP signal was detected with an
710 emitting wavelength of 488 nm and a detection window of 500 – 545 nm. The RFP signal was excited
711 with 561 nm and detected between 650 nm and 695 nm. To compare the fluorescence signal close to
712 the penetration site with signal in unpenetrated areas, zoomed in Z-stacks with identical settings were
713 taken at both locations. The fluorescence intensities and GFP/RFP ratios were determined using Fiji
714 Image J.

715 **Co-IP MS/MS**

716 Five week-old FER-GFP and Lti6b-GFP plants were infected with powdery mildew and harvested,
717 together with untreated samples at 24 h post infection. Per genotype and treatment, the rosettes of 12
718 plants were harvested and ground in liquid nitrogen. All plant material was used for further protein
719 extraction. Proteins were extracted with 1 ml extraction buffer (50 mM TRIS-HCl pH 7,5, 100 mM NaCl,
720 10 % glycerol, 2mM EDTA, 2mM DTT, 1 % protease inhibitor cocktail, 1 % PMSF, 1% IGEPAL) per 1
721 ml plant material. For immunoprecipitation, GFP-Trap agarose beads (ChromoTek) were used and
722 incubated with the crude extract for 3 h at 4 °C. Beads were washed 3 times with wash buffer (50 mM
723 Tris-HCl pH 7.5, 50 mM NaCl, 1 mM phenylmethanesulfonyl fluoride, 0.1 % IGEPAL). Subsequently,
724 washed beads were incubated in 50 µL of Laemmli sample buffer for 10 min at 95 °C. Next, in-gel trypsin
725 digestion was performed according to standard procedures (Shevchenko et al., 2006). Briefly, samples
726 were run on a Nu-PAGE™ 4%–12% Bis-Tris protein gel (ThermoFisher Scientific) for about 1 cm.
727 Subsequently, the still not size-separated single protein band per sample was cut out, reduced (50mM
728 dithiothreitol), alkylated (55mm chloroacetamide) and digested overnight with trypsin (Trypsin Gold,
729 mass spectrometry grade, Promega). The peptides obtained were dried to completeness and
730 resuspended in 24 µL of 2% acetonitrile, 0.1% formic acid in HPLC grade water. Finally, 5 µL of sample
731 were injected per mass spectrometric (MS) measurement.

732 LC-MS/MS data acquisition was carried out on a Dionex Ultimate 3000 RSLCnano system coupled to a
733 Q-Exactive HF-X mass spectrometer (ThermoFisher Scientific, Bremen). Peptides were delivered to a
734 trap column (ReproSil-pur C18-AQ, 5 µm, Dr. Maisch, 20 mm × 75 µm, self-packed) at a flow rate of 5
735 µL/min in 0.1% formic acid in HPLC grade water. After 10 minutes of loading, peptides were transferred
736 to an analytical column (ReproSil Gold C18-AQ, 3 µm, Dr. Maisch, 450 mm × 75 µm, self-packed) and
737 separated using a 50 min gradient from 4% to 32% of solvent B (0.1% FA, 5% DMSO in acetonitrile) in
738 solvent A (0.1% FA, 5% DMSO in HPLC grade water) at 300 nL/min flow rate. The Q-Exactive HF-X
739 mass spectrometer was operated in data dependent acquisition (DDA) and positive ionization mode.
740 MS1 spectra (360–1300 m/z) were recorded at a resolution of 60k using an automatic gain control (AGC)
741 target value of 3 e^6 and maximum injection time (maxIT) of 45 msec. Up to 18 peptide precursors were
742 selected for fragmentation. Only precursors with charge state 2 to 6 were selected and dynamic
743 exclusion of 30 sec was enabled. Peptide fragmentation was performed using higher energy collision
744 induced dissociation (HCD) and a normalized collision energy (NCE) of 26%. The precursor isolation
745 window width was set to 1.3 m/z. MS2 Resolution was 15.000 with an automatic gain control (AGC)
746 target value of $1e^5$ and maximum injection time (maxIT) of 25 msec.

747 Protein and phosphopeptide identification and quantification were performed using the software
748 MaxQuant (version 1.6.3.4) (Tyanova et al., 2016) with its built-in search engine Andromeda. MS2
749 spectra were searched against the TAIR *Arabidopsis thaliana* protein database (downloaded March
750 2022, 48231 protein entries) supplemented with the GFP protein sequence as well as with common
751 contaminants (built-in option in MaxQuant). Trypsin/P was specified as proteolytic enzyme.
752 Carbamidomethylated cysteine was set as fixed modification. Phosphorylation of
753 serine/threonine/tyrosine, oxidation of methionine and acetylation at the protein N-terminus were
754 specified as variable modifications. Results were adjusted to a 1% false discovery rate on peptide
755 spectrum match (PSM) level and protein level employing a target-decoy approach using reversed
756 protein sequences. The minimal peptide length was defined as 7 amino acids and the "match-between-
757 run" functionality was enabled (matching time window 0.7 min, alignment time window 20 min). For
758 protein quantification the MaxQuant output table proteinGroups.txt and Label-Free Quantification (LFQ)
759 (Cox et al., 2014) intensities were used. Only proteins detected in at least two biological replicates in at
760 least one experimental condition were further processed. Missing values were imputed by a protein-
761 specific constant value, which was defined as the lowest detected protein-specific LFQ-value over all
762 samples divided by two, using the data visualisation platform omicsViewer (DOI:
763 10.1101/2022.03.10.483845). Additionally, a maximal imputed LFQ value was defined as 15% quantile
764 of the protein distribution from the dataset. The volcano plots (Figure S4A, S5A) were generated using
765 RStudio. Interactions were marked as significant if they passed the threshold of FDR < 0.05 and fold
766 change > 2. For phosphopeptide detection the MaxQuant output table Phospho(STY)Sites.txt was used.
767 Only phosphosites detected on FERONIA in at least two biological replicates in at least one experimental
768 condition were considered. The FER-GFP infected with powdery mildew and untreated experiments
769 were performed in biological triplicates, while all other experiments were performed in biological
770 quadruplets.

771 **Petiole length measurements**

772 Petioles were measured from rosettes of 4 week-old plants. Individual plants were cut off from the root
773 and leaves were detached close to the base. Individual leaves were imaged, and petiole length was
774 quantified using Fiji ImageJ software.

775 **Identification of putative powdery mildew RALF-likes**

776 To identify putative RALF-like peptides in the predicted proteins and genome assemblies of selected
777 phytopathogenic fungi, we used the hmmsearch program from the hmmer suite v3.3.2 (www.hmmer.org)
778 with default parameters. The hidden markov model profile (.hmm) for the RALF motif (PF05498.15) was
779 obtained from the PFAM website (https://ftp.ebi.ac.uk/pub/databases/Pfam/current_release/Pfam-
780 A.hmm.gz), access data 19.11.2023). The RALF HMM profile was used to search predicted protein
781 sequences from the selected fungal species (see Supplementary Table X) using the hmmsearch
782 function. Hits with E-values below $1e^{-05}$ were retained. To perform the hmmsearch analysis on the
783 genome assemblies, we used a custom Python script to split the contigs into 300 bp fragments with a
784 sliding window of 50bp. All six open reading frames of these split sequences were translated, and stop
785 codons were removed to generate a multi-FASTA file suitable for be processed with hmmsearch. Search

786 hits with E-values < 1e-05 were retained. Accession number of genome assemblies used in this analysis
787 are reported in Supplementary Table S1.

788 **Quantification and statistical analysis**

789 GraphPad Prism (Version 8.0.1) was used to perform statistical analysis. Detailed descriptions of the
790 sample size, p-values and statistical methods are indicated in the respective figure legends.

791 **Funding**

792 This work was funded by the following agencies: Deutsche Forschungsgemeinschaft (DFG) grants
793 STE2448/4-1 (HL and MS), TRR356 TP B09 (HL, SS and MS), EN 1071/3-1 (TE) and the Technical
794 University of Munich (MS, HL, SS, MM, RH).

795 **Author contributions**

796 Conceptualization: MS; Investigation: HL, MS, SS, JH, KM, MM, TL, GH; Funding acquisition: MS, RH,
797 JH, TE, TK; Project administration: MS; Supervision: MS, HL, TE, JH, RH; Writing – original draft: HL,
798 MS; Writing – review & editing: SS, MM, KM, TK, TE, JH, RH.

799 **Acknowledgements**

800 We thank Stefanie Ranf for providing GoldenGate vectors for molecular cloning and Mark Youles (TSL
801 Norwich) and Laurence Tomlinson (TSL Norwich) for providing the pICSL4723OD vector for CRISPR-
802 Cas9 cloning. We thank Hannah König for supporting the collection of micrographs to assess callose
803 depositions in rosette leaves and trichomes. The authors thank Verena Breitner and Franziska
804 Hackbarth for excellent technical assistance and maintenance of mass spectrometers at the BayBioMS.
805 The Q Exactive HFX mass spectrometer was funded in part by the German Research Foundation (INST
806 95/1435-1 FUGG).

807 **Declaration of interests**

808 The authors declare no competing interests.

809 **Data availability**

810 The mass spectrometric raw files as well as the MaxQuant output files have been deposited to the
811 ProteomeXchange Consortium via the PRIDE partner repository and can be accessed using the
812 identifier PXD059737 (https://proteomecentral.proteomexchange.org/cgi/GetDataset?ID=PXD059737).
813 Reviewer account username: reviewer_pxd059737@ebi.ac.uk, password: lumM0fo5d8wq.

814

References

Abarca, A., Franck, C.M., and Zipfel, C. (2021). Family-wide evaluation of RAPID ALKALINIZATION FACTOR peptides. Plant Physiology **187**:996-1010. doi:10.1093/plphys/kiab308.

Acevedo-Garcia, J., Spencer, D., Thieron, H., Reinstädler, A., Hammond-Kosack, K., Phillips, A.L., and Panstruga, R. (2017). mlo-based powdery mildew resistance in hexaploid bread wheat generated by a non-transgenic TILLING approach. Plant Biotechnology Journal **15**:367-378. doi:10.1111/pbi.12631.

Baunsgaard, L., Fuglsang, A.T., Jahn, T., Korthout, H.A.A.J., De Boer, A.H., and Palmgren, M.G. (1998). The 14–3-3 proteins associate with the plant plasma membrane H1-ATPase to generate a fusicoccin binding complex and a fusicoccin responsive system. The Plant Journal **13**:661-671. doi:10.1046/j.1365-313X.1998.00083.x.

Bethke, G., Grundman, R.E., Sreekanta, S., Truman, W., Katagiri, F., and Glazebrook, J. (2014). Arabidopsis PECTIN METHYLESTERASEs contribute to immunity against Pseudomonas syringae. Plant Physiol **164**:1093-1107. doi:10.1104/pp.113.227637.

Bezrutczyk, M., Yang, J., Eom, J.-S., Prior, M., Sosso, D., Hartwig, T., Szurek, B., Oliva, R., Vera-Cruz, C., White, F.F., et al. (2018). Sugar flux and signaling in plant–microbe interactions. The Plant Journal **93**:675-685. doi:10.1111/tpj.13775.

Bhat, R.A., Miklis, M., Schmelzer, E., Schulze-Lefert, P., and Panstruga, R. (2005). Recruitment and interaction dynamics of plant penetration resistance components in a plasma membrane microdomain. Proceedings of the National Academy of Sciences **102**:3135-3140. doi:10.1073/pnas.0500012102.

Biermann, D., von Arx, M., Xhelilaj, K., Séré, D., Stegmann, M., Wolf, S., Zipfel, C., and Gronnier, J. (2024). A RALF-Brassinosteroid morpho-signaling circuit regulates *Arabidopsis* hypocotyl cell shape. bioRxiv:2024.2003.2028.587199. doi:10.1101/2024.03.28.587199.

Bürger, M., and Chory, J. (2019). Stressed Out About Hormones: How Plants Orchestrate Immunity. Cell Host & Microbe **26**:163-172. doi:10.1016/j.chom.2019.07.006.

Büschges, R., Hollricher, K., Panstruga, R., Simons, G., Wolter, M., Frijters, A., van Daelen, R., van der Lee, T., Diergaarde, P., Groenendijk, J., et al. (1997). The Barley *Mlo* Gene: A Novel Control Element of Plant Pathogen Resistance. Cell **88**:695-705. doi:10.1016/S0092-8674(00)81912-1.

Castel, B., Tomlinson, L., Locci, F., Yang, Y., and Jones, J.D.G. (2019). Optimization of T-DNA architecture for Cas9-mediated mutagenesis in Arabidopsis. PLOS ONE **14**:e0204778. doi:10.1371/journal.pone.0204778.

Chakravorty, D., Yu, Y., and Assmann, S.M. (2018). A kinase-dead version of FERONIA receptor-like kinase has dose-dependent impacts on rosette morphology and RALF1-mediated stomatal movements. FEBS Letters **592**:3429-3437. doi:10.1002/1873-3468.13249.

Chen, J., Xu, F., Qiang, X., Liu, H., Wang, L., Jiang, L., Li, C., Wang, B., Luan, S., Wu, D., et al. (2024). Regulated cleavage and translocation of FERONIA control immunity in Arabidopsis roots. Nature Plants **10**:1761-1774. doi:10.1038/s41477-024-01823-8.

Collins, N.C., Thordal-Christensen, H., Lipka, V., Bau, S., Kombrink, E., Qiu, J.-L., Hückelhoven, R., Stein, M., Freialdenhoven, A., Somerville, S.C., et al. (2003). SNARE-protein-mediated disease resistance at the plant cell wall. Nature **425**:973-977. doi:10.1038/nature02076.

Consonni, C., Humphry, M.E., Hartmann, H.A., Livaja, M., Durner, J., Westphal, L., Vogel, J., Lipka, V., Kemmerling, B., Schulze-Lefert, P., et al. (2006). Conserved requirement for a plant host cell protein in powdery mildew pathogenesis. Nat Genet **38**:716-720. doi:10.1038/ng1806.

Cox, J., Hein, M.Y., Luber, C.A., Paron, I., Nagaraj, N., and Mann, M. (2014). Accurate Proteome-wide Label-free Quantification by Delayed Normalization and Maximal Peptide Ratio Extraction, Termed MaxLFQ*. Molecular & Cellular Proteomics **13**:2513-2526. doi:10.1074/mcp.M113.031591.

Delulio, G.A., Guo, L., Zhang, Y., Goldberg, J.M., Kistler, H.C., and Ma, L.-J. (2018). Kinome Expansion in the Fusarium oxysporum Species Complex Driven by Accessory Chromosomes. mSphere **3**:10.1128/msphere.00231-00218. doi:10.1128/msphere.00231-18.

Del Corpo, D., Fullone, M.R., Miele, R., Lafond, M., Pontiggia, D., Grisel, S., Kieffer-Jaquinod, S., Giardina, T., Bellincampi, D., and Lionetti, V. (2020). AtPME17 is a functional Arabidopsis thaliana pectin methylesterase regulated by its PRO region that triggers PME activity in the resistance to Botrytis cinerea. Molecular Plant Pathology **21**:1620-1633. doi:10.1111/mpp.13002.

Deslauriers, S.D., and Larsen, P.B. (2010). FERONIA Is a Key Modulator of Brassinosteroid and Ethylene Responsiveness in Arabidopsis Hypocotyls. Molecular Plant **3**:626-640. doi:10.1093/mp/ssq015.

Dobón, A., Canet, J.V., García-Andrade, J., Angulo, C., Neumetzler, L., Persson, S., and Vera, P. (2015). Novel Disease Susceptibility Factors for Fungal Necrotrophic Pathogens in Arabidopsis. PLOS Pathogens **11**:e1004800. doi:10.1371/journal.ppat.1004800.

Douchkov, D., Lück, S., Johrde, A., Nowara, D., Himmelbach, A., Rajaraman, J., Stein, N., Sharma, R., Kilian, B., and Schweizer, P. (2014). Discovery of genes affecting resistance of barley to adapted and non-adapted powdery mildew fungi. Genome Biology **15**:518. doi:10.1186/s13059-014-0518-8.

Draeger, C., Ndinyanka Fabrice, T., Gineau, E., Mouille, G., Kuhn, B.M., Moller, I., Abdou, M.T., Frey, B., Pauly, M., Bacic, A., et al. (2015). Arabidopsis leucine-rich repeat extensin (LRX) proteins modify cell wall composition and influence plant growth. BMC Plant Biol **15**:155. doi:10.1186/s12870-015-0548-8.

Du, C., Li, X., Chen, J., Chen, W., Li, B., Li, C., Wang, L., Li, J., Zhao, X., Lin, J., et al. (2016). Receptor kinase complex transmits RALF peptide signal to inhibit root growth in *Arabidopsis*. Proceedings of the National Academy of Sciences **113**:E8326-E8334. doi:10.1073/pnas.1609626113.

Duan, Q., Kita, D., Li, C., Cheung, A.Y., and Wu, H.-M. (2010). FERONIA receptor-like kinase regulates RHO GTPase signaling of root hair development. Proceedings of the National Academy of Sciences **107**:17821-17826. doi:10.1073/pnas.1005366107.

Dünser, K., Gupta, S., Herger, A., Feraru, M.I., Ringli, C., and Kleine-Vehn, J. (2019). Extracellular matrix sensing by FERONIA and Leucine Rich Repeat Extensins controls vacuolar expansion during cellular elongation in Arabidopsis thaliana. The EMBO Journal **38**:e100353. doi:10.15252/embj.2018100353.

Engelhardt, S., Stam, R., and Hückelhoven, R. (2018). Good Riddance? Breaking Disease Susceptibility in the Era of New Breeding Technologies. Agronomy **8**:114. doi:10.3390/agronomy8070114

Engelsdorf, T., Gigli-Bisceglia, N., Veerabagu, M., McKenna, J.F., Vaahtera, L., Augstein, F., Van der Does, D., Zipfel, C., and Hamann, T. (2018). The plant cell wall integrity maintenance and immune signaling systems cooperate to control stress responses in Arabidopsis thaliana. Science Signaling **11**:eaao3070. doi:10.1126/scisignal.aao3070.

Fabrice, T.N., Vogler, H., Draeger, C., Munglani, G., Gupta, S., Herger, A.G., Knox, P., Grossniklaus, U., and Ringli, C. (2018). LRX Proteins Play a Crucial Role in Pollen Grain and Pollen Tube Cell Wall Development. Plant Physiol **176**:1981-1992. doi:10.1104/pp.17.01374.

Falhof, J., Pedersen, Jesper T., Fuglsang, Anja T., and Palmgren, M. (2016). Plasma Membrane H+-ATPase Regulation in the Center of Plant Physiology. Molecular Plant **9**:323-337. doi:10.1016/j.molp.2015.11.002.

Felle, H.H., Herrmann, A., Hanstein, S., Hückelhoven, R., and Kogel, K.-H. (2004). Apoplastic pH Signaling in Barley Leaves Attacked by the Powdery Mildew Fungus Blumeria graminis f. sp. hordei. Molecular Plant-Microbe Interactions® **17**:118-123. doi:10.1094/mpmi.2004.17.1.118.

Fotopoulos, V., Gilbert, M.J., Pittman, J.K., Marvier, A.C., Buchanan, A.J., Sauer, N., Hall, J.L., and Williams, L.E. (2003). The monosaccharide transporter gene, AtSTP4, and the cell-wall invertase, Atbetafruct1, are induced in Arabidopsis during infection with the fungal biotroph Erysiphe cichoracearum. Plant Physiol **132**:821-829. doi:10.1104/pp.103.021428.

Galindo-Trigo, S., Blanco-Touriñán, N., DeFalco, T.A., Wells, E.S., Gray, J.E., Zipfel, C., and Smith, L.M. (2020). *Cr*RLK1L receptor-like kinases HERK1 and ANJEA are female determinants of pollen tube reception. EMBO reports **21**:e48466. doi:10.15252/embr.201948466.

Gao, Q., Wang, C., Xi, Y., Shao, Q., Li, L., and Luan, S. (2022). A receptor–channel trio conducts Ca2+ signalling for pollen tube reception. Nature **607**:534-539. doi:10.1038/s41586-022-04923-7.

Ge, Z., Bergonci, T., Zhao, Y., Zou, Y., Du, S., Liu, M.-C., Luo, X., Ruan, H., García-Valencia, L.E., Zhong, S., et al. (2017). Arabidopsis pollen tube integrity and sperm release are regulated by RALF-mediated signaling. Science **358**:1596-1600. doi:10.1126/science.aao3642.

Geiger, D. (2020). Plant glucose transporter structure and function. Pflügers Archiv - European Journal of Physiology **472**:1111-1128. doi:10.1007/s00424-020-02449-3.

Glawe, D.A. (2008). The Powdery Mildews: A Review of the World's Most Familiar (Yet Poorly Known) Plant Pathogens. Annual Review of Phytopathology **46**:27-51. doi:10.1146/annurev.phyto.46.081407.104740.

Gonneau, M., Desprez, T., Martin, M., Doblas, V.G., Bacete, L., Miart, F., Sormani, R., Hématy, K., Renou, J., Landrein, B., et al. (2018). Receptor Kinase THESEUS1 Is a Rapid Alkalinization Factor 34 Receptor in Arabidopsis. Current Biology **28**:2452-2458.e2454. doi:10.1016/j.cub.2018.05.075.

Gronnier, J., Franck, C.M., Stegmann, M., DeFalco, T.A., Abarca, A., von Arx, M., Dünser, K., Lin, W., Yang, Z., Kleine-Vehn, J., et al. (2022). Regulation of immune receptor kinase plasma membrane nanoscale organization by a plant peptide hormone and its receptors. eLife **11**:e74162. doi:10.7554/eLife.74162.

Guénin, S., Mareck, A., Rayon, C., Lamour, R., Assoumou Ndong, Y., Domon, J.-M., Sénéchal, F., Fournet, F., Jamet, E., Canut, H., et al. (2011). Identification of pectin methylesterase 3 as a basic pectin methylesterase isoform involved in adventitious rooting in Arabidopsis thaliana. New Phytologist **192**:114-126. doi:10.1111/j.1469-8137.2011.03797.x.

Guo, H., Nolan, T.M., Song, G., Liu, S., Xie, Z., Chen, J., Schnable, P.S., Walley, J.W., and Yin, Y. (2018). FERONIA Receptor Kinase Contributes to Plant Immunity by Suppressing Jasmonic Acid Signaling in *Arabidopsis thaliana*. Current Biology **28**:3316-3324.e3316. doi:10.1016/j.cub.2018.07.078.

Harholt, J., Suttangkakul, A., and Vibe Scheller, H. (2010). Biosynthesis of Pectin. Plant Physiology **153**:384-395. doi:10.1104/pp.110.156588.

Haruta, M., Sabat, G., Stecker, K., Minkoff, B.B., and Sussman, M.R. (2014). A Peptide Hormone and Its Receptor Protein Kinase Regulate Plant Cell Expansion. Science **343**:408-411. doi:10.1126/science.1244454.

Haruta, M., Gaddameedi, V., Burch, H., Fernandez, D., and Sussman, M.R. (2018). Comparison of the effects of a kinase-dead mutation of FERONIA on ovule fertilization and root growth of Arabidopsis. FEBS Letters **592**:2395-2402. doi:10.1002/1873-3468.13157.

Haruta, M., Burch, H.L., Nelson, R.B., Barrett-Wilt, G., Kline, K.G., Mohsin, S.B., Young, J.C., Otegui, M.S., and Sussman, M.R. (2010). Molecular Characterization of Mutant Arabidopsis Plants with Reduced Plasma Membrane Proton Pump Activity Journal of Biological Chemistry **285**:17918-17929. doi:10.1074/jbc.M110.101733.

Hayashi, Y., Nakamura, S., Takemiya, A., Takahashi, Y., Shimazaki, K.-i., and Kinoshita, T. (2010). Biochemical Characterization of In Vitro Phosphorylation and Dephosphorylation of the Plasma Membrane H+-ATPase. Plant and Cell Physiology **51**:1186-1196. doi:10.1093/pcp/pcq078.

Herger, A., Gupta, S., Kadler, G., Franck, C.M., Boisson-Dernier, A., and Ringli, C. (2020). Overlapping functions and protein-protein interactions of LRR-extensins in Arabidopsis. PLOS Genetics **16**:e1008847. doi:10.1371/journal.pgen.1008847.

Hocq, L., Sénéchal, F., Lefebvre, V., Lehner, A., Domon, J.-M., Mollet, J.-C., Dehors, J., Pageau, K., Marcelo, P., Guérineau, F., et al. (2016). Combined Experimental and Computational Approaches Reveal Distinct pH Dependence of Pectin Methylesterase Inhibitors. Plant Physiology **173**:1075-1093. doi:10.1104/pp.16.01790.

Hocq, L., Habrylo, O., Sénéchal, F., Voxeur, A., Pau-Roblot, C., Safran, J., Fournet, F., Bassard, S., Battu, V., Demailly, H., et al. (2023). Mutation of AtPME2, a pH-Dependent Pectin Methylesterase, Affects Cell Wall Structure and Hypocotyl Elongation. Plant and Cell Physiology **65**:301-318. doi:10.1093/pcp/pcad154.

Hok, S., Danchin, E.G.J., Allasia, V., Panabières, F., Attard, A., and Keller, H. (2011). An Arabidopsis (malectin-like) leucine-rich repeat receptor-like kinase contributes to downy mildew disease. Plant, Cell & Environment **34**:1944-1957. doi:10.1111/j.1365-3040.2011.02390.x.

Hok, S., Allasia, V., Andrio, E., Naessens, E., Ribes, E., Panabières, F., Attard, A., Ris, N., Clément, M., Barlet, X., et al. (2014). The Receptor Kinase IMPAIRED OOMYCETE SUSCEPTIBILITY1 Attenuates Abscisic Acid Responses in Arabidopsis Plant Physiology **166**:1506-1518. doi:10.1104/pp.114.248518.

Huang, Y., Yin, C., Liu, J., Feng, B., Ge, D., Kong, L., Ortiz-Morea, F.A., Richter, J., Hauser, M.-T., Wang, W.-M., et al. (2020). A trimeric CrRLK1L-LLG1 complex genetically modulates SUMM2-mediated autoimmunity. Nature Communications **11**:4859. doi:10.1038/s41467-020-18600-8.

Hückelhoven, R., and Panstruga, R. (2011). Cell biology of the plant–powdery mildew interaction. Current Opinion in Plant Biology **14**:738-746. doi:10.1016/j.pbi.2011.08.002.

Huebbers, J.W., Caldarescu, G.A., Kubátová, Z., Sabol, P., Levecque, S.C.J., Kuhn, H., Kulich, I., Reinstädler, A., Büttgen, K., Manga-Robles, A., et al. (2024). Interplay of EXO70 and MLO proteins modulates trichome cell wall composition and susceptibility to powdery mildew. The Plant Cell **36**:1007-1035. doi:10.1093/plcell/koad319.

Kadota, Y., Sklenar, J., Derbyshire, P., Stransfeld, L., Asai, S., Ntoukakis, V., Jones, Jonathan D., Shirasu, K., Menke, F., Jones, A., et al. (2014). Direct Regulation of the NADPH Oxidase RBOHD by the PRR-Associated Kinase BIK1 during Plant Immunity. Molecular Cell **54**:43-55. doi:10.1016/j.molcel.2014.02.021.

Kessler, S.A., Shimosato-Asano, H., Keinath, N.F., Wuest, S.E., Ingram, G., Panstruga, R., and Grossniklaus, U. (2010). Conserved Molecular Components for Pollen Tube Reception and Fungal Invasion. Science **330**:968-971. doi:10.1126/science.1195211.

Kesten, C., Gámez-Arjona, F.M., Menna, A., Scholl, S., Dora, S., Huerta, A.I., Huang, H.Y., Tintor, N., Kinoshita, T., Rep, M., et al. (2019). Pathogen induced pH changes regulate the growth defense balance in plants. The EMBO Journal **38**:e101822. doi:10.15252/embj.2019101822.

Kusch, S., and Panstruga, R. (2017). mlo-Based Resistance: An Apparently Universal "Weapon" to Defeat Powdery Mildew Disease. Molecular Plant-Microbe Interactions® **30**:179-189. doi:10.1094/mpmi-12-16-0255-cr.

Lan, Z., Song, Z., Wang, Z., Li, L., Liu, Y., Zhi, S., Wang, R., Wang, J., Li, Q., Bleckmann, A., et al. (2023). Antagonistic RALF peptides control an intergeneric hybridization barrier on Brassicaceae stigmas. Cell **186**:4773-4787.e4712. doi:10.1016/j.cell.2023.09.003.

Levesque-Tremblay, G., Pelloux, J., Braybrook, S.A., and Müller, K. (2015). Tuning of pectin methylesterification: consequences for cell wall biomechanics and development. Planta **242**:791-811. doi:10.1007/s00425-015-2358-5.

Lewis, K.C., Selzer, T., Shahar, C., Udi, Y., Tworowski, D., and Sagi, I. (2008). Inhibition of pectin methyl esterase activity by green tea catechins. Phytochemistry **69**:2586-2592. doi:10.1016/j.phytochem.2008.08.012.

Li, C., Yeh, F.-L., Cheung, A.Y., Duan, Q., Kita, D., Liu, M.-C., Maman, J., Luu, E.J., Wu, B.W., Gates, L., et al. (2015). Glycosylphosphatidylinositol-anchored proteins as chaperones and co-receptors for FERONIA receptor kinase signaling in Arabidopsis. eLife **4**:e06587. doi:10.7554/eLife.06587.

Li, L., Chen, H., Alotaibi, S.S., Pěnčík, A., Adamowski, M., Novák, O., and Friml, J. (2022a). RALF1 peptide triggers biphasic root growth inhibition upstream of auxin biosynthesis. Proceedings of the National Academy of Sciences **119**:e2121058119. doi:10.1073/pnas.2121058119.

Li, S., Lin, D., Zhang, Y., Deng, M., Chen, Y., Lv, B., Li, B., Lei, Y., Wang, Y., Zhao, L., et al. (2022b). Genome-edited powdery mildew resistance in wheat without growth penalties. Nature **602**:455-460. doi:10.1038/s41586-022-04395-9.

Lin, W., Tang, W., Pan, X., Huang, A., Gao, X., Anderson, C.T., and Yang, Z. (2022). *Arabidopsis* pavement cell morphogenesis requires FERONIA binding to pectin for activation of ROP GTPase signaling. Current Biology **32**:497-507.e494. doi:10.1016/j.cub.2021.11.030.

Lin, W., Zhou, X., Tang, W., Takahashi, K., Pan, X., Dai, J., Ren, H., Zhu, X., Pan, S., Zheng, H., et al. (2021). TMK-based cell-surface auxin signalling activates cell-wall acidification. Nature **599**:278-282. doi:10.1038/s41586-021-03976-4.

Liu, C., Yu, H., Voxeur, A., Rao, X., and Dixon, R.A. (2023). FERONIA and wall-associated kinases coordinate defense induced by lignin modification in plant cell walls. Science Advances **9**:eadf7714. doi:10.1126/sciadv.adf7714.

Liu, J., Liu, M., Tan, L., Huai, B., Ma, X., Pan, Q., Zheng, P., Wen, Y., Zhang, Q., Zhao, Q., et al. (2021). AtSTP8, an endoplasmic reticulum-localised monosaccharide transporter from Arabidopsis, is recruited to the extrahaustorial membrane during powdery mildew infection. New Phytologist **230**:2404-2419. doi:10.1111/nph.17347.

Liu, J., Huang, Y., Kong, L., Yu, X., Feng, B., Liu, D., Zhao, B., Mendes, G.C., Yuan, P., Ge, D., et al. (2020). The malectin-like receptor-like kinase LETUM1 modulates NLR protein SUMM2 activation via MEKK2 scaffolding. Nature Plants **6**:1106-1115. doi:10.1038/s41477-020-0748-6.

Liu, M.-C.J., Yeh, F.-L.J., Yvon, R., Simpson, K., Jordan, S., Chambers, J., Wu, H.-M., and Cheung, A.Y. (2024). Extracellular pectin-RALF phase separation mediates FERONIA global signaling function. Cell **187**:312-330.e322. doi:10.1016/j.cell.2023.11.038.

Liu, S., Bartnikas, L.M., Volko, S.M., Ausubel, F.M., and Tang, D. (2016). Mutation of the Glucosinolate Biosynthesis Enzyme Cytochrome P450 83A1 Monooxygenase Increases Camalexin Accumulation and Powdery Mildew Resistance. Frontiers in Plant Science **7**doi:10.3389/fpls.2016.00227.

Liu, Z., Chu, X., Ren, W., Cheng, L., Liu, C., Wang, C., Gao, S., Dai, S., and Li, C. (2025). PCP-B peptides and CrRLK1L receptor kinases control pollination via pH gating of aquaporins in Arabidopsis. Developmental Cell doi:10.1016/j.devcel.2024.12.026.

Mang, H., Feng, B., Hu, Z., Boisson-Dernier, A., Franck, C.M., Meng, X., Huang, Y., Zhou, J., Xu, G., Wang, T., et al. (2017). Differential Regulation of Two-Tiered Plant Immunity and Sexual Reproduction by ANXUR Receptor-Like Kinases. The Plant Cell **29**:3140-3156. doi:10.1105/tpc.17.00464.

Manning, V.A., Pandelova, I., Dhillon, B., Wilhelm, L.J., Goodwin, S.B., Berlin, A.M., Figueroa, M., Freitag, M., Hane, J.K., Henrissat, B., et al. (2013). Comparative Genomics of a Plant-Pathogenic Fungus, Pyrenophora tritici-repentis, Reveals Transduplication and the Impact of Repeat Elements on Pathogenicity and Population Divergence. G3 Genes|Genomes|Genetics **3**:41-63. doi:10.1534/g3.112.004044.

Masachis, S., Segorbe, D., Turrà, D., Leon-Ruiz, M., Fürst, U., El Ghalid, M., Leonard, G., López-Berges, M.S., Richards, T.A., Felix, G., et al. (2016). A fungal pathogen secretes plant alkalinizing peptides to increase infection. Nature Microbiology **1**:16043. doi:10.1038/nmicrobiol.2016.43.

Mecchia, M.A., Santos-Fernandez, G., Duss, N.N., Somoza, S.C., Boisson-Dernier, A., Gagliardini, V., Martínez-Bernardini, A., Fabrice, T.N., Ringli, C., Muschietti, J.P., et al. (2017). RALF4/19 peptides interact with LRX proteins to control pollen tube growth in Arabidopsis. Science **358**:1600-1603. doi:10.1126/science.aao5467.

Merlot, S., Leonhardt, N., Fenzi, F., Valon, C., Costa, M., Piette, L., Vavasseur, A., Genty, B., Boivin, K., Müller, A., et al. (2007). Constitutive activation of a plasma membrane H+ATPase prevents abscisic acid-mediated stomatal closure. The EMBO Journal **26**:3216-3226. doi:10.1038/sj.emboj.7601750.

Micali, C., Göllner, K., Humphry, M., Consonni, C., and Panstruga, R. (2008). The Powdery Mildew Disease of Arabidopsis: A Paradigm for the Interaction between Plants and Biotrophic Fungi. Arabidopsis Book **6**:e0115. doi:10.1199/tab.0115.

Micali, C.O., Neumann, U., Grunewald, D., Panstruga, R., and O'Connell, R. (2011). Biogenesis of a specialized plant–fungal interface during host cell internalization of Golovinomyces orontii haustoria. Cellular Microbiology **13**:210-226. doi:10.1111/j.1462-5822.2010.01530.x.

Milne, R.J., Dibley, K.E., Schnippenkoetter, W., Mascher, M., Lui, A.C.W., Wang, L., Lo, C., Ashton, A.R., Ryan, P.R., and Lagudah, E.S. (2019). The Wheat Lr67 Gene from the Sugar Transport Protein 13 Family Confers Multipathogen Resistance in Barley. Plant Physiol **179**:1285-1297. doi:10.1104/pp.18.00945.

Moussu, S., Broyart, C., Santos-Fernandez, G., Augustin, S., Wehrle, S., Grossniklaus, U., and Santiago, J. (2020). Structural basis for recognition of RALF peptides by LRX proteins during pollen tube growth. Proceedings of the National Academy of Sciences **117**:7494-7503. doi:10.1073/pnas.2000100117.

Moussu, S., Lee, H.K., Haas, K.T., Broyart, C., Rathgeb, U., De Bellis, D., Levasseur, T., Schoenaers, S., Fernandez, G.S., Grossniklaus, U., et al. (2023). Plant cell wall patterning and expansion mediated by protein-peptide-polysaccharide interaction. Science **382**:719-725. doi:10.1126/science.adi4720.

Mucha, S., Heinzlmeir, S., Kriechbaumer, V., Strickland, B., Kirchhelle, C., Choudhary, M., Kowalski, N., Eichmann, R., Hückelhoven, R., Grill, E., et al. (2019). The Formation of a Camalexin Biosynthetic Metabolon. The Plant Cell **31**:2697-2710. doi:10.1105/tpc.19.00403.

Müller, M.C., Praz, C.R., Sotiropoulos, A.G., Menardo, F., Kunz, L., Schudel, S., Oberhänsli, S., Poretti, M., Wehrli, A., Bourras, S., et al. (2019). A chromosome-scale genome assembly reveals a highly dynamic effector repertoire of wheat powdery mildew. New Phytologist **221**:2176-2189. doi:10.1111/nph.15529.

Nawrath, C., and Métraux, J.-P. (1999). Salicylic Acid Induction–Deficient Mutants of Arabidopsis Express PR-2 and PR-5 and Accumulate High Levels of Camalexin after Pathogen Inoculation. The Plant Cell **11**:1393-1404. doi:10.1105/tpc.11.8.1393.

Nekrasov, V., Wang, C., Win, J., Lanz, C., Weigel, D., and Kamoun, S. (2017). Rapid generation of a transgene-free powdery mildew resistant tomato by genome deletion. Scientific Reports **7**:482. doi:10.1038/s41598-017-00578-x.

Ngou, B.P.M., Jones, J.D.G., and Ding, P. (2022). Plant immune networks. Trends in Plant Science **27**:255-273. doi:10.1016/j.tplants.2021.08.012.

Nishimura, M.T., Stein, M., Hou, B.-H., Vogel, J.P., Edwards, H., and Somerville, S.C. (2003). Loss of a Callose Synthase Results in Salicylic Acid-Dependent Disease Resistance. Science **301**:969-972. doi:10.1126/science.1086716.

Noble, J.A., Bielski, N.V., Liu, M.-C.J., DeFalco, T.A., Stegmann, M., Nelson, A.D.L., McNamara, K., Sullivan, B., Dinh, K.K., Khuu, N., et al. (2022). Evolutionary analysis of the LORELEI gene family in plants reveals regulatory subfunctionalization. Plant Physiology **190**:2539-2556. doi:10.1093/plphys/kiac444.

Pearce, G., Yamaguchi, Y., Munske, G., and Ryan, C.A. (2010). Structure–activity studies of RALF, Rapid Alkalinization Factor, reveal an essential – YISY – motif. Peptides **31**:1973-1977. doi:10.1016/j.peptides.2010.08.012.

Peaucelle, A., Louvet, R., Johansen, J.N., Höfte, H., Laufs, P., Pelloux, J., and Mouille, G. (2008). Arabidopsis Phyllotaxis Is Controlled by the Methyl-Esterification Status of Cell-Wall Pectins. Current Biology **18**:1943-1948. doi:10.1016/j.cub.2008.10.065.

Pelloux, J., Rustérucci, C., and Mellerowicz, E.J. (2007). New insights into pectin methylesterase structure and function. Trends in Plant Science **12**:267-277. doi:10.1016/j.tplants.2007.04.001.

Peng, Y., Yang, J., Li, X., and Zhang, Y. (2021). Salicylic Acid: Biosynthesis and Signaling. Annual Review of Plant Biology **72**:761-791. doi:10.1146/annurev-arplant-081320-092855.

Polonio, Á., Pérez-García, A., Martínez-Cruz, J., Fernández-Ortuño, D., and de Vicente, A. (2021). The Haustorium of Phytopathogenic Fungi: A Short Overview of a Specialized Cell of Obligate Biotrophic Plant Parasites. In Progress in Botany Vol. 82, F.M. Cánovas and U. Lüttge and

M.-C. Risueño and H. Pretzsch, eds. (Springer International Publishing: Cham), pp. 337-355. doi:10.1007/124_2020_45.

Ried, M.K., Banhara, A., Hwu, F.-Y., Binder, A., Gust, A.A., Höfle, C., Hückelhoven, R., Nürnberger, T., and Parniske, M. (2019). A set of Arabidopsis genes involved in the accommodation of the downy mildew pathogen Hyaloperonospora arabidopsidis. PLOS Pathogens **15**:e1007747. doi:10.1371/journal.ppat.1007747.

Rößling, A.-K., Dünser, K., Liu, C., Lauw, S., Rodriguez-Franco, M., Kalmbach, L., Barbez, E., and Kleine-Vehn, J. (2024). Pectin methylesterase activity is required for RALF1 peptide signalling output. eLife **13**:RP96943. doi:10.7554/eLife.96943.

Rzemieniewski, J., and Stegmann, M. (2022). Regulation of pattern-triggered immunity and growth by phytocytokines. Current Opinion in Plant Biology **68**:102230. doi:10.1016/j.pbi.2022.102230.

Schmid, M., Davison, T.S., Henz, S.R., Pape, U.J., Demar, M., Vingron, M., Schölkopf, B., Weigel, D., and Lohmann, J.U. (2005). A gene expression map of Arabidopsis thaliana development. Nat Genet **37**:501-506. doi:10.1038/ng1543.

Schnepf, V., Vlot, A.C., Kugler, K., and Hückelhoven, R. (2018). Barley susceptibility factor RACB modulates transcript levels of signalling protein genes in compatible interaction with Blumeria graminis f.sp. hordei. Molecular Plant Pathology **19**:393-404. doi:10.1111/mpp.12531.

Schoenaers, S., Lee, H.K., Gonneau, M., Faucher, E., Levasseur, T., Akary, E., Claeijs, N., Moussu, S., Broyart, C., Balcerowicz, D., et al. (2024). Rapid alkalinization factor 22 has a structural and signalling role in root hair cell wall assembly. Nature Plants **10**:494-511. doi:10.1038/s41477-024-01637-8.

Sénéchal, F., Habrylo, O., Hocq, L., Domon, J.-M., Marcelo, P., Lefebvre, V., Pelloux, J., and Mercadante, D. (2017). Structural and dynamical characterization of the pH-dependence of the pectin methylesterase-pectin methylesterase inhibitor complex. Journal of Biological Chemistry **292**:21538-21547. doi:10.1074/jbc.RA117.000197.

Shen, Q., Bourdais, G., Pan, H., Robatzek, S., and Tang, D. (2017). *Arabidopsis* glycosylphosphatidylinositol-anchored protein LLG1 associates with and modulates FLS2 to regulate innate immunity. Proceedings of the National Academy of Sciences **114**:5749-5754. doi:10.1073/pnas.1614468114.

Shevchenko, A., Tomas, H., Havli, J., Olsen, J.V., and Mann, M. (2006). In-gel digestion for mass spectrometric characterization of proteins and proteomes. Nature Protocols **1**:2856-2860. doi:10.1038/nprot.2006.468.

Stegmann, M., Monaghan, J., Smakowska-Luzan, E., Rovenich, H., Lehner, A., Holton, N., Belkhadir, Y., and Zipfel, C. (2017). The receptor kinase FER is a RALF-regulated scaffold controlling plant immune signaling. Science **355**:287-289. doi:10.1126/science.aal2541.

Stein, M.n., Dittgen, J., Sánchez-Rodríguez, C., Hou, B.-H., Molina, A., Schulze-Lefert, P., Lipka, V., and Somerville, S. (2006). Arabidopsis PEN3/PDR8, an ATP Binding Cassette Transporter, Contributes to Nonhost Resistance to Inappropriate Pathogens That Enter by Direct Penetration. The Plant Cell **18**:731-746. doi:10.1105/tpc.105.038372.

Takahashi, K., Hayashi, K.-i., and Kinoshita, T. (2012). Auxin Activates the Plasma Membrane H+-ATPase by Phosphorylation during Hypocotyl Elongation in Arabidopsis Plant Physiology **159**:632-641. doi:10.1104/pp.112.196428.

Tang, J., Wu, D., Li, X., Wang, L., Xu, L., Zhang, Y., Xu, F., Liu, H., Xie, Q., Dai, S., et al. (2022). Plant immunity suppression via PHR1-RALF-FERONIA shapes the root microbiome to alleviate phosphate starvation. The EMBO Journal **41**:e109102. doi:10.15252/embj.2021109102.

Thynne, E., Saur, I.M.L., Simbaqueba, J., Ogilvie, H.A., Gonzalez-Cendales, Y., Mead, O., Taranto, A., Catanzariti, A.-M., McDonald, M.C., Schwessinger, B., et al. (2017). Fungal phytopathogens encode functional homologues of plant rapid alkalinization factor (RALF) peptides. Molecular Plant Pathology **18**:811-824. doi:10.1111/mpp.12444.

Tyanova, S., Temu, T., and Cox, J. (2016). The MaxQuant computational platform for mass spectrometry-based shotgun proteomics. Nature Protocols **11**:2301-2319. doi:10.1038/nprot.2016.136.

van Schie, C.C.N., and Takken, F.L.W. (2014). Susceptibility Genes 101: How to Be a Good Host. Annual Review of Phytopathology **52**:551-581. doi:10.1146/annurev-phyto-102313-045854.

Voegele, R.T., and Mendgen, K.W. (2011). Nutrient uptake in rust fungi: how sweet is parasitic life? Euphytica **179**:41-55. doi:10.1007/s10681-011-0358-5.

Vogel, J.P., Raab, T.K., Schiff, C., and Somerville, S.C. (2002). PMR6, a Pectate Lyase–Like Gene Required for Powdery Mildew Susceptibility in Arabidopsis. The Plant Cell **14**:2095-2106. doi:10.1105/tpc.003509.

Weis, C., Pfeilmeier, S., Glawischnig, E., Isono, E., Pachl, F., Hahne, H., Kuster, B., Eichmann, R., and Hückelhoven, R. (2013). Co-immunoprecipitation-based identification of putative BAX INHIBITOR-1-interacting proteins involved in cell death regulation and plant–powdery mildew interactions. Molecular Plant Pathology **14**:791-802. doi:10.1111/mpp.12050.

Wiese, J., Kranz, T., and Schubert, S. (2004). Induction of Pathogen Resistance in Barley by Abiotic Stress. Plant Biol (Stuttg) **6**:529-536. doi:10.1055/s-2004-821176.

Willats, W.G.T., Orfila, C., Limberg, G., Buchholt, H.C., van Alebeek, G.-J.W.M., Voragen, A.G., Marcus, S.E., Christensen, T.M.I.E., Mikkelsen, J.D., Murray, B.S., et al. (2001). Modulation of the Degree and Pattern of Methyl-esterification of Pectic Homogalacturonan in Plant Cell Walls: IMPLICATIONS FOR PECTIN METHYL ESTERASE ACTION, MATRIX PROPERTIES, AND CELL ADHESION Journal of Biological Chemistry **276**:19404-19413. doi:10.1074/jbc.M011242200.

Wormit, A., and Usadel, B. (2018). The Multifaceted Role of Pectin Methylesterase Inhibitors (PMEIs). International Journal of Molecular Sciences **19**:2878.

Wu, Y., Ma, X., Pan, Z., Kale, S.D., Song, Y., King, H., Zhang, Q., Presley, C., Deng, X., Wei, C.-I., et al. (2018). Comparative genome analyses reveal sequence features reflecting distinct modes of host-adaptation between dicot and monocot powdery mildew. BMC Genomics **19**:705. doi:10.1186/s12864-018-5069-z.

Xiao, Y., Stegmann, M., Han, Z., DeFalco, T.A., Parys, K., Xu, L., Belkhadir, Y., Zipfel, C., and Chai, J. (2019). Mechanisms of RALF peptide perception by a heterotypic receptor complex. Nature **572**:270-274. doi:10.1038/s41586-019-1409-7.

Xu, F., Gonneau, M., Faucher, E., Habrylo, O., Lefebvre, V., Domon, J.-M., Martin, M., Sénéchal, F., Peaucelle, A., Pelloux, J., et al. (2022). Biochemical characterization of Pectin Methylesterase Inhibitor 3 from Arabidopsis thaliana. The Cell Surface **8**:100080. doi:10.1016/j.tcsw.2022.100080.

Xu, X., and Chen, X. (2023). A complete genome sequence of Podosphaera xanthii race 2 F, the causal agent of powdery mildew isolated from cucumber in China. figshare.

Yamada, K., Saijo, Y., Nakagami, H., and Takano, Y. (2016). Regulation of sugar transporter activity for antibacterial defense in Arabidopsis. Science **354**:1427-1430. doi:10.1126/science.aah5692.

Yang, T., Wang, L., Li, C., Liu, Y., Zhu, S., Qi, Y., Liu, X., Lin, Q., Luan, S., and Yu, F. (2015). Receptor protein kinase FERONIA controls leaf starch accumulation by interacting with glyceraldehyde-3-phosphate dehydrogenase. Biochemical and Biophysical Research Communications **465**:77-82. doi:10.1016/j.bbrc.2015.07.132.

Yeats, T.H., Sorek, H., Wemmer, D.E., and Somerville, C.R. (2016). Cellulose Deficiency Is Enhanced on Hyper Accumulation of Sucrose by a H+-Coupled Sucrose Symporter Plant Physiology **171**:110-124. doi:10.1104/pp.16.00302.

Zaccaron, A.Z., Neill, T., Corcoran, J., Mahaffee, W.F., and Stergiopoulos, I. (2023). A chromosome-scale genome assembly of the grape powdery mildew pathogen *Erysiphe necator* reveals its genomic architecture and previously unknown features of its biology. mBio **14**:e00645-00623. doi:10.1128/mbio.00645-23.

Zhang, K., Halitschke, R., Yin, C., Liu, C.-J., and Gan, S.-S. (2013). Salicylic acid 3-hydroxylase regulates *Arabidopsis* leaf longevity by mediating salicylic acid catabolism. Proceedings of the National Academy of Sciences **110**:14807-14812. doi:10.1073/pnas.1302702110.

Zhang, X., Peng, H., Zhu, S., Xing, J., Li, X., Zhu, Z., Zheng, J., Wang, L., Wang, B., Chen, J., et al. (2020). Nematode-Encoded RALF Peptide Mimics Facilitate Parasitism of Plants through the FERONIA Receptor Kinase. Molecular Plant **13**:1434-1454. doi:10.1016/j.molp.2020.08.014.

Zhang, Y., Zhao, L., Zhao, J., Li, Y., Wang, J., Guo, R., Gan, S., Liu, C.-J., and Zhang, K. (2017). S5H/DMR6 Encodes a Salicylic Acid 5-Hydroxylase That Fine-Tunes Salicylic Acid Homeostasis Plant Physiology **175**:1082-1093. doi:10.1104/pp.17.00695.

Zhao, C., Zayed, O., Yu, Z., Jiang, W., Zhu, P., Hsu, C.-C., Zhang, L., Tao, W.A., Lozano-Durán, R., and Zhu, J.-K. (2018). Leucine-rich repeat extensin proteins regulate plant salt tolerance in *Arabidopsis*. Proceedings of the National Academy of Sciences **115**:13123-13128. doi:10.1073/pnas.1816991115.

Zhong, S., Li, L., Wang, Z., Ge, Z., Li, Q., Bleckmann, A., Wang, J., Song, Z., Shi, Y., Liu, T., et al. (2022). RALF peptide signaling controls the polytubey block in Arabidopsis. Science **375**:290-296. doi:10.1126/science.abl4683.

Zhou, F., Andersen, C.H., Burhenne, K., Fischer, P.H., Collinge, D.B., and Thordal-Christensen, H. (2000). Proton extrusion is an essential signalling component in the HR of epidermal single cells in the barley-powdery mildew interaction. Plant J **23**:245-254. doi:10.1046/j.1365-313x.2000.00777.x.

Zhu, S., Fu, Q., Xu, F., Zheng, H., and Yu, F. (2021). New paradigms in cell adaptation: decades of discoveries on the CrRLK1L receptor kinase signalling network. New Phytologist **232**:1168-1183. doi:10.1111/nph.17683.

Zimmerli, L., Stein, M., Lipka, V., Schulze-Lefert, P., and Somerville, S. (2004). Host and non-host pathogens elicit different jasmonate/ethylene responses in Arabidopsis. The Plant Journal **40**:633-646. doi:10.1111/j.1365-313X.2004.02236.x.

1257 **Figures**

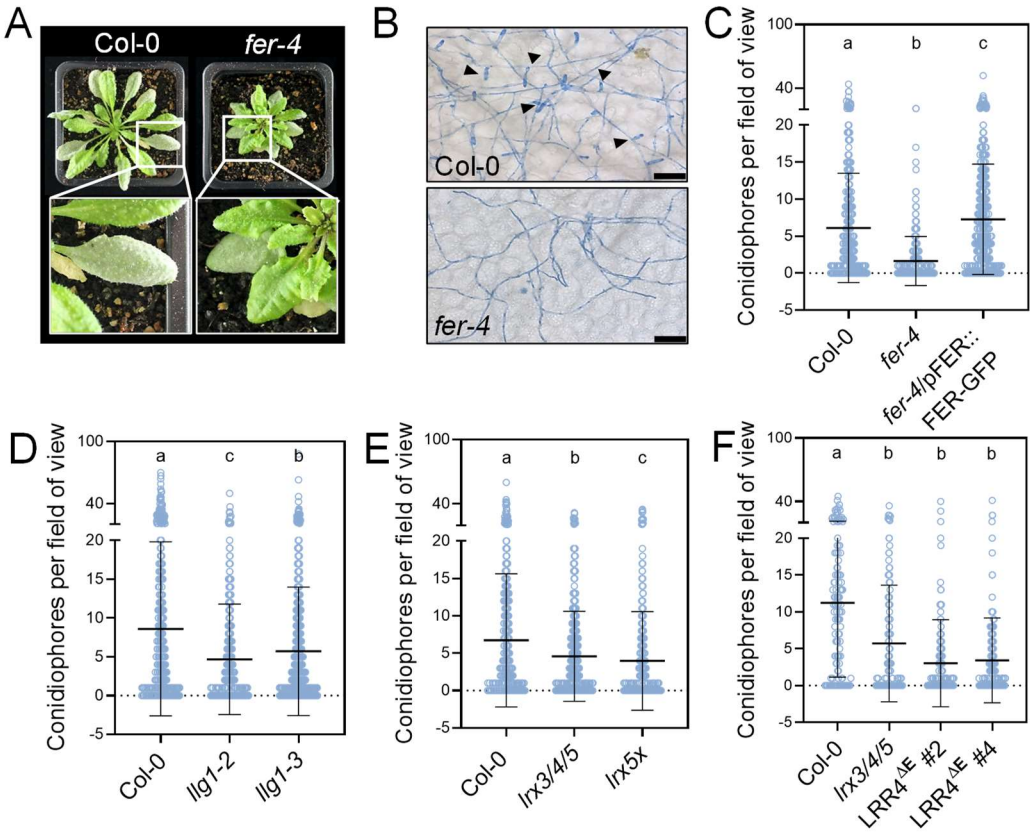

1258

1259 **Figure 1: FER and additional RALF binding proteins are *Ecr* susceptibility factors.** A) Images of
1260 Col-0 and *fer-4* plants infected with *Ecr* (14 dpi). B) Ink stained *Ecr* colonies (5 dpi) grown on Col-0 and
1261 *fer-4* plants. Black arrows indicate conidiophores. Scale bar represents 50 µm. C) Conidiophores per
1262 field of view (5 dpi) of fungal colonies grown upon *Ecr* infection of the indicated genotypes. Mean ± SD,
1263 n=223-392 pooled from three independent experiments (Dunn's multiple comparisons test, a-b, b-c
1264 $p<0.0001$; a-c $p=0.0106$). D) Conidiophores per field of view (5 dpi) of fungal colonies grown upon *Ecr*
1265 infection of the indicated genotypes. Mean ± SD, n=345-665 pooled from five independent experiments
1266 (Dunn's multiple comparisons test, a-b, a-c $p<0.0001$; b-c $p=0.0235$). E) Conidiophores per field of view
1267 (5 dpi) of fungal colonies grown upon *Ecr* infection of the indicated genotypes. Mean ± SD, n=285-453
1268 pooled from three independent experiments (Dunn's multiple comparisons test, a-b $p=0.0150$; a-c
1269 $p<0.0001$; b-c $p=0.0408$). F) Conidiophores per field of view (5 dpi) of fungal colonies grown upon *Ecr*
1270 infection of the indicated genotypes. Mean ± SD, n=113-159 pooled from two independent experiments
1271 (Dunn's multiple comparisons test, a-b $p<0.0001$). All experiments were done at least three times with
1272 similar results, except (F), which was repeated once with identical results.

1273

1274

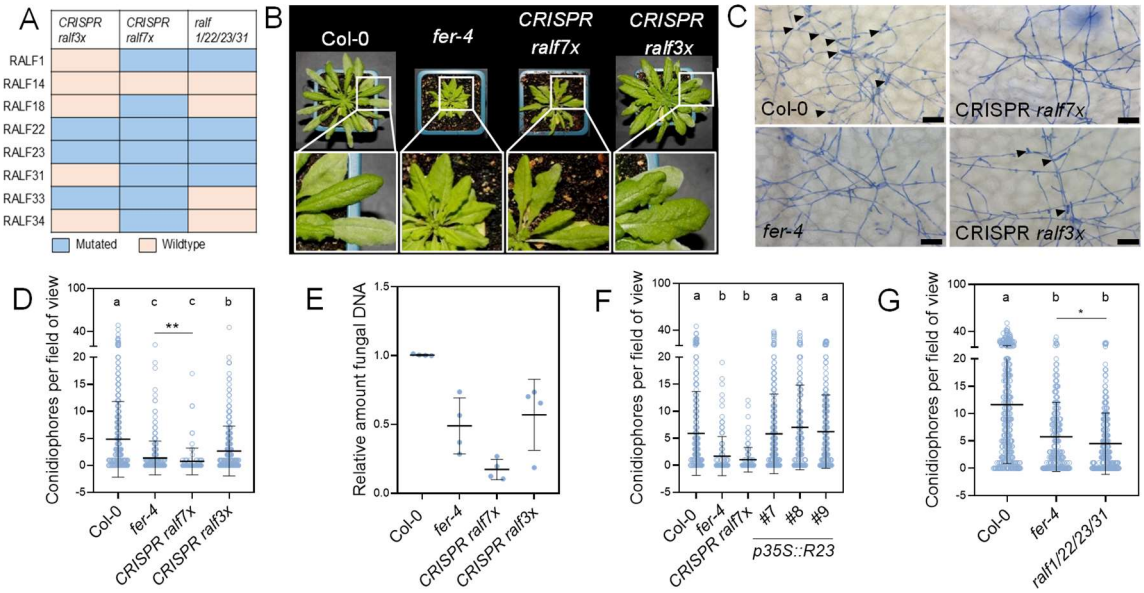

1275

1276 **Figure 2: Specific RALFs are powdery mildew susceptibility factors.** A) Table of RALF peptides
1277 mutated in CRISPR *ralf3x*, CRISPR *ralf7x* and *ralf1/22/23/31* B) Images of Col-0*, fer-4*, CRISPR *ralf3x*
1278 and CRISPR *ralf7x* plants infected with *Ecr* (14 dpi). C) Ink stained *Ecr* colonies (5 dpi) grown on Col-0,
1279 *fer-4*, CRISPR *ralf3x* and CRISPR *ralf7x* plants. Black arrows indicate conidiophores. Scale bar
1280 represents 50 µm. D) Conidiophores per field of view (5 dpi) of fungal colonies grown upon *Ecr* infection
1281 of the indicated genotypes. Mean ± SD, n=98-456 pooled from three independent experiments (Dunn's
1282 multiple comparisons test, a-b, a-c $p<0.0001$, b-c $p<0.0002$. Comparison between *fer-4* and CRISPR
1283 *ralf7x*: Mann Whitney test, ** $p=0.007$). E) Amount of fungal DNA normalized to plant DNA (5 dpi) upon
1284 *Ecr* infection of the indicated genotypes. Mean ± SD, n=4, data points indicate independent biological
1285 replicates. F) Conidiophores per field of view (5 dpi) of fungal colonies grown upon *Ecr* infection of the
1286 indicated genotypes. Mean ± SD, n=101-286 pooled from three independent experiments (Dunn's
1287 multiple comparisons test, a-b $p<0.0001$). G) Conidiophores per field of view (5 dpi) of fungal colonies
1288 grown upon *Ecr* infection of the indicated genotypes. Mean ± SD, n=226-382 pooled from three
1289 independent experiments (Dunn's multiple comparisons test, a-b $p<0.0001$. Comparison between *fer-4*
1290 and*ralf1/22/23/31*: Mann Whitney test, ** $p=0.0132$). All experiments were done at least three times with
1291 similar results.

1292

1293

1294

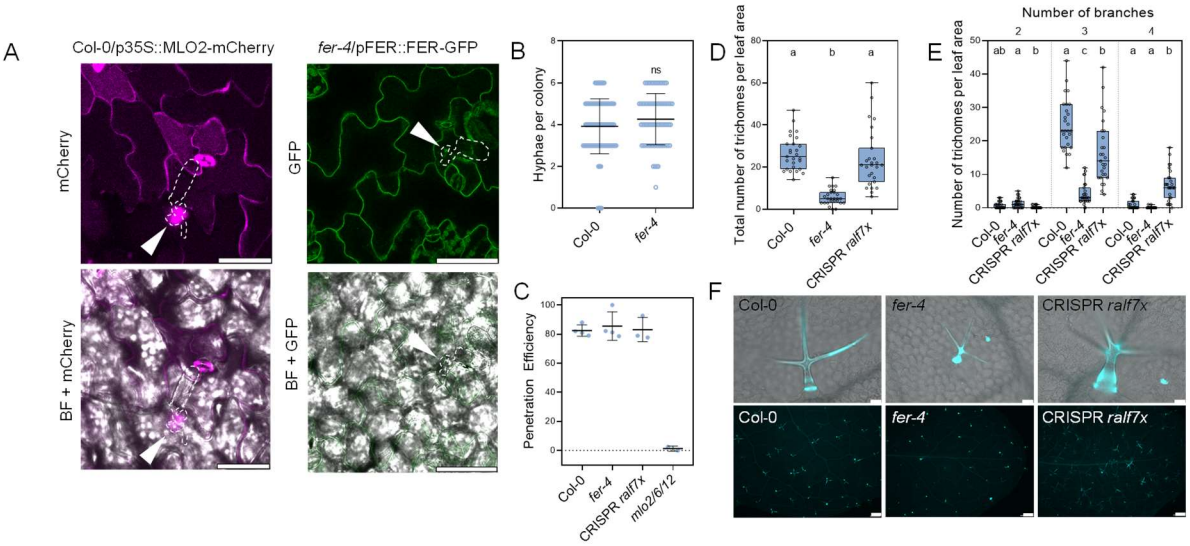

1295

1296 **Figure 3: FER and RALF mediated powdery mildew susceptibility is most likely not directly linked**
1297 **to MLO.** A) Confocal microscopy images of fungal spores penetrating p35S::MLO2-mCherry and
1298 pFER::FER-GFP lines (2 dpi). Dotted lines indicate fungal spores, white arrow marks the penetration
1299 site. Scale bar represents 50 µm. B) Quantification of hyphal branching (2 dpi). Mean ± SD, n=77–98
1300 pooled from two independent experiments (Mann Whitney test, ns: not significant). C) Penetration
1301 efficiency of *Ecr* on the indicated genotypes (calculated as the percentage of successful penetrations
1302 from all counted interactions, 2 dpi). Mean ± SD, n=2–4. D) Quantification of trichome numbers per leaf
1303 area on the indicated genotypes. Mean ± SD, n=27 pooled from three independent experiments (Dunn's
1304 multiple comparisons test, a-b $p<0.0001$). E) Quantification of trichome branching on the indicated
1305 genotypes. Mean ± SD, n=27 pooled from three independent experiments (Dunn's multiple comparisons
1306 test, statistical analysis was performed on each category individually, 2 branches: a-b $p=0.0002$; 3
1307 branches: a-b $p=0.0259$; a-c, b-c $p<0.0001$; 4 branches: a-b $p<0.0001$). F) Microscopic images of aniline
1308 blue-stained trichomes of Col-0, *fer-4* and CRISPR *ralf7x*. Scale bar in the upper row represents 50 µm,
1309 scale bar in the lower panel represents 500 µm. All experiments were done three times with similar
1310 results, except (B), which was repeated once with identical results.

1311

1312

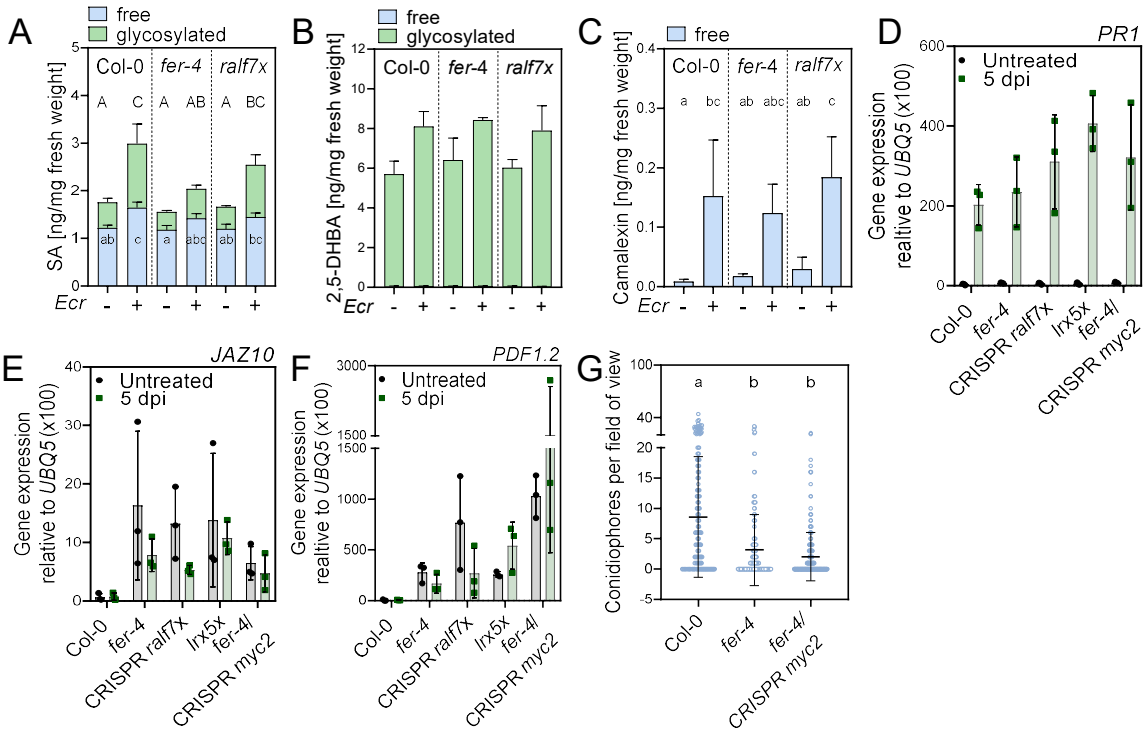

Figure 4: FER-RALF mediated powdery mildew susceptibility is independent of JA and SA signaling. A) Quantification of free (blue) and glycosylated (green) SA in untreated and *Ecr* infected (5 dpi) leaves of the indicated genotypes. Mean ± SD, n=3 pooled from three independent experiments (Tukey's multiple comparisons test, free and glycosylated SA was analysed individually, free: a-bc p=0.0423; a-c p=0.0006; ab-c p≤0.0013, glycosylated: A-C p≤0.0029; A-BC p≤0.0383) B) Quantification of free (blue) and glycosylated (green) 2,5-DHBA in untreated and *Ecr* infected (5 dpi) leaves of the indicated genotypes. Mean ± SD, n=3 pooled from three independent experiments (Tukey's multiple comparisons test, all comparisons were not significant) C) Quantification of free (blue) Camalexin in untreated and *Ecr* infected (5 dpi) leaves of the indicated genotypes. Mean ± SD, n=3 pooled from three independent experiments (Tukey's multiple comparisons test, a-bc p=0.0486; ab-c p≤0.0319; a-c p=0.0137. D) RT-qPCR of *PR1* in untreated (grey) adult leaves and upon infection with *Ecr* (5 dpi, green). Housekeeping gene *UBQ5*. Mean ± SD, n=3, data points indicate independent biological replicates. E) RT-qPCR of *JAZ10* in untreated (grey) adult leaves and upon infection with *Ecr* (5 dpi, green). Housekeeping gene *UBQ5*. Mean ± SD, n=3, data points indicate independent biological replicates. F) RT-qPCR of *PDF1.2* in untreated (grey) adult leaves and upon infection with *Ecr* (5 dpi, green). Housekeeping gene *UBQ5*. Mean ± SD, n=3, data points indicate independent biological replicates. G) Conidiophores per field of view (5 dpi) of fungal colonies grown upon *Ecr* infection of the indicated genotypes. Mean ± SD, n=152-209 pooled from three independent experiments (Dunn's multiple comparisons test, a-b p<0.0001). All experiments were done three times with similar results.

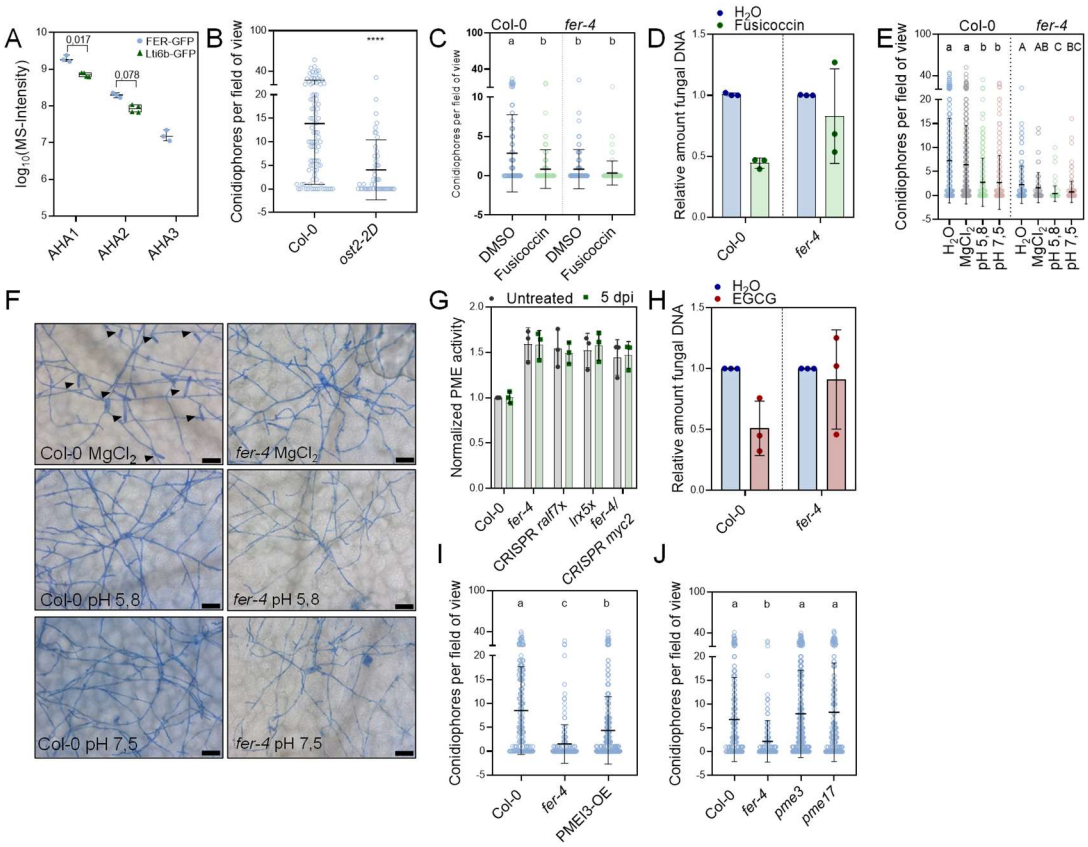

Figure 5: Apoplastic pH modulation and PME activity determine powdery mildew infection success. A) MS Intensities measured after Co-immunoprecipitation with untreated pFER::FER-GFP and p35S::Lti6b-GFP plants using GFP-TRAP beads. n=3 for pFER::FER-GFP, n=4 for p35S::Lti6b-GFP, data points indicate independent biological replicates. FDR values indicate statistical differences between pFER::FER-GFP and p35S::Lti6b-GFP. No AHA3 derived peptides were detected in p35S::Lti6b-GFP samples. B) Conidiophores per field of view (5 dpi) of fungal colonies grown upon *Ecr* infection of the indicated genotypes. Mean ± SD, n=49-91 pooled from two independent experiments (Mann Whitney test, ****p<0.0001). C) Conidiophores per field of view (5 dpi) of fungal colonies grown upon *Ecr* infection of leaves pretreated with H_2O (blue) or Fusicoccin (green). Mean ± SD, n=71-113 pooled from four independent experiments (Dunn's multiple comparisons test, a-b p≤0.0008). D) Amount of fungal DNA normalized to plant DNA (5 dpi) upon *Ecr* infection and pretreatment with H_2O (blue) or Fusicoccin (green). Mean ± SD, n=3, data points indicate independent biological replicates. E) Conidiophores per field of view (5 dpi) after pretreatment with H_2O (blue), $MgCl_2$ 15 mM pH 5.8 (grey), MES buffer 10 mM pH 5.8 (green) and MES buffer 10 mM pH 7.5 (red) before *Ecr* infection. Mean ± SD, n=52-347 pooled from four independent experiments (Dunn's multiple comparisons test, a-b p<0,005, A-B p=0.0381, B-C p=0.0015, A-C p<0.0001). F) Ink stained *Ecr* colonies (5 dpi) grown on Col-0 and *fer-4* plants after pretreatment with 15 mM $MgCl_2$, 10 mM MES buffer (pH 5.8) and 10 mM MES buffer (pH 7.5). Black arrows indicate conidiophores. Scale bar represents 50 µm. F) PME activity in untreated leaves (grey) and upon *Ecr* infection (5 dpi, green) normalized to Col-0 PME activity in untreated leaves. Mean ± SD, n=3, data points indicate independent biological replicates. G) Amount of fungal DNA normalized to plant DNA (5 dpi) upon *Ecr* infection and pretreatment with H_2O (blue) or EGCG (red). Mean ± SD, n=3, data points indicate independent biological replicates. H) Conidiophores per field of view (5 dpi) of fungal colonies grown upon *Ecr* infection of the indicated genotypes. Mean ± SD, n=182-309 pooled from four independent experiments (Dunn's multiple comparisons test, a-b, b-c, a-c p<0.0001). I) Conidiophores per field of view (5 dpi) of fungal colonies grown upon *Ecr* infection of the indicated genotypes. Mean ± SD, n=161-338 pooled from three independent experiments (Dunn's multiple comparisons test, a-b p<0.0001). All experiments were done at least three times with similar results.

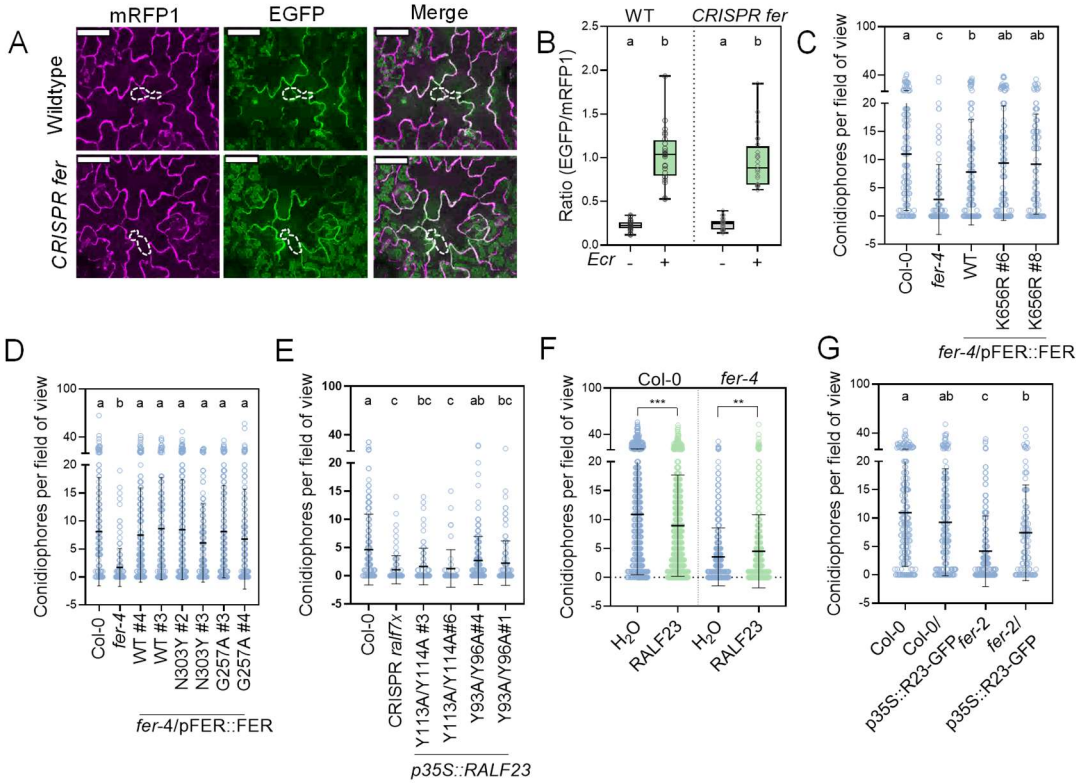

Figure 6: RALF-mediated powdery mildew susceptibility is partially independent of FER and FER signaling. A) Confocal images of pUBQ10::SYP122-pHusion lines in the Col-0 and CRISPR *fer* background (2 dpi). Dotted lines indicate the location of the fungal spore. Scale bar represents 50 µm. B) Quantification of the EGFP/mRFP1 ratio near the penetration site (green) and in uninfected areas (grey). Mean ± SD, n=24 pooled from three independent experiments (Mann Whitney test, a-b p<0.0001). C) Conidiophores per field of view (5 dpi) of fungal colonies grown upon *Ecr* infection of the indicated genotypes. Mean ± SD, n=95-137 pooled from three independent experiments (Dunn's multiple comparisons test, a-b p=0.0277, a-c p<0.0001). D) Conidiophores per field of view (5 dpi) of fungal colonies grown upon *Ecr* infection of the indicated genotypes. Mean ± SD, n=131-210 pooled from four independent experiments (Dunn's multiple comparisons test, a-b p<0.0001). E) Conidiophores per field of view (5 dpi) of fungal colonies grown upon *Ecr* infection of the indicated genotypes. Mean ± SD, n=48-189 pooled from two independent experiments (Dunn's multiple comparisons test, a-bc p≤0.0031, ab-c ≤0,0049, a-c<0.0001). F) Conidiophores per field of view (5 dpi) after pretreatment with H_2O (blue) or 1µM RALF23 before *Ecr* infection. Mean ± SD, n=485-970 pooled from 11 independent experiments (Mann Whitney test, statistical analysis was performed on each genotype individually, Col-0: ***p=0.0008, *fer-4* ** p=0.0064). G) Conidiophores per field of view (5 dpi) of fungal colonies grown upon *Ecr* infection of the indicated genotypes. Mean ± SD, n=95 - 137 pooled from 3 independent experiments (Dunn's multiple comparisons test, a-b p=0.0076, a-c p<0.0001, b-c p=0.0017). All experiments were done at least three times with similar results.

1383 **Supplemental Figures**

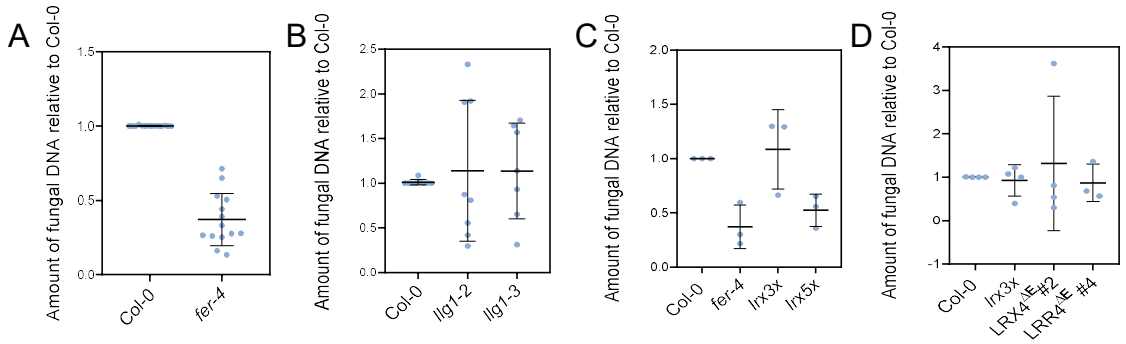

1384

1385 **Figure S1: Quantification of fungal growth on mutants of RALF binding proteins.** A – D) Amount
1386 of fungal DNA normalized to plant DNA (5 dpi) upon *Ecr* infection of the indicated genotypes. Mean ±
1387 SD, data points indicate independent biological replicates A) n=14, B) n=7–9, C) n=3, D) n =3–4. All
1388 experiments were done at least three times with similar results.

1389

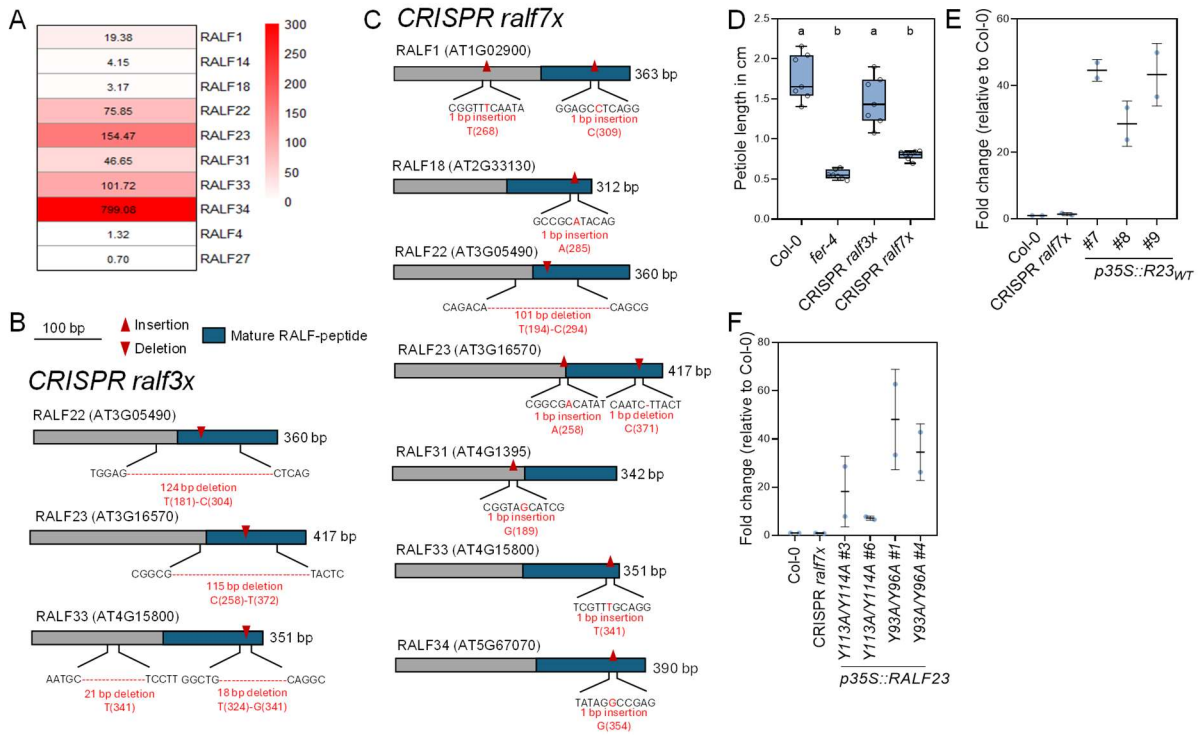

Figure S2: Characterization of CRISPR *ralf* mutants. A) Expression levels of the indicated *RALF* genes in the vegetative rosette. Data was obtained using ePlant browser (https://bar.utoronto.ca/eplant/) and is based on (Schmid et al., 2005). B) Characterization of CRISPR *ralf3x*. Schematic diagram of *RALF22, RALF23* and *RALF33* gene structure and the CRISPR-Cas9-mediated mutation pattern detected by DNA sequencing. The mature RALF peptide is indicated in blue. C) Characterization of CRISPR *ralf7x*. Schematic diagram of *RALF1, RALF18, RALF22, RALF31, RALF23*, *RALF33* and *RALF34* gene structure and the CRISPR-Cas9-mediated mutation pattern detected by DNA sequencing. The mature RALF peptide is indicated in blue. D) Quantification of the petiole length of 5 week-old Col-0, *fer*-4, CRISPR *ralf3x* and CRISPR *ralf7x* plants. Each data point represents the average length of petioles on a fully grown rosette. Mean ± SD, n=7 pooled from two independent experiments (Tukey's multiple comparisons test, a-b $p<0.0001$). E – F) RT-qPCR of *RALF23* in adult leaves of the indicated plant lines. Housekeeping gene *UBQ5*. Mean ± SD, n=2, data points indicate independent biological replicates. E) – F) were repeated once with identical results.

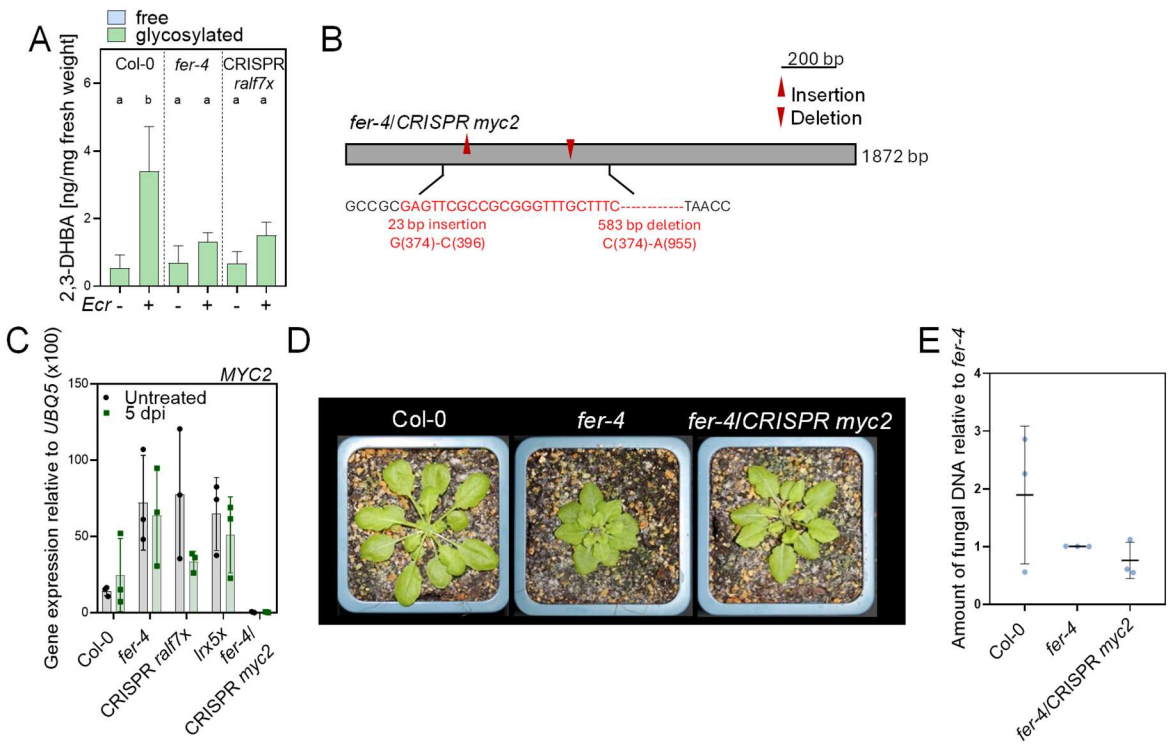

Figure S3: Characterization of *fer*-4 CRISPR *myc2.* A) Quantification of free (blue) and glycosylated (green) 2,3-DHBA in untreated and *Ecr* infected (5 dpi) leaves of the indicated genotypes. Mean ± SD, n=3 pooled from three independent experiments (Tukey's multiple comparisons test, glycosylated: a-b p≤0.0324). (B) Characterization of *fer-4* CRISPR *myc2*. Schematic diagram of *MYC2* gene structure and the CRISPR-Cas9-mediated mutation pattern detected by DNA sequencing. C) RT-qPCR of *MYC2* in untreated (grey) adult leaves and upon infection with *Ecr* (5 dpi, green). Housekeeping gene *UBQ5*. Mean ± SD, n=3, data points indicate independent biological replicates. (D) Images of 4 week-old Col-0, *fer-4* and *fer-4* CRISPR *myc2* plants. (D) Amount of fungal DNA normalized to plant DNA (5 dpi) upon *Ecr* infection of the indicated genotypes. Mean ± SD, n=3, data points indicate independent biological replicates. A), C) and E) were done three times with similar results.

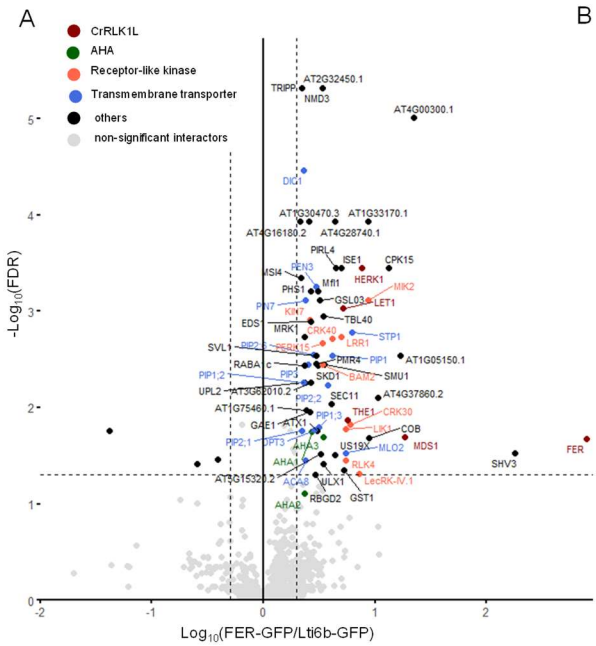

B

Identifier	Molecular function	FDR	log(10)FC
AT3G51550.1 FER	Receptor kinase	0,0212	2,899
AT5G38990.1 MDS1	Receptor kinase	0,0200	1,274
AT3G46290.1 HERK1	Receptor kinase	0,0004	0,880
AT5G54380.1 THE1	Receptor kinase	0,0136	0,751
AT2G23200.1 LET1	Receptor kinase	0,0009	0,715
AT2G37710.1 LecRK-IV.1	Receptor kinase	0,0487	0,855
AT4G08850.1 MIK2	Receptor kinase	0,0008	0,941
AT4G23180.1 RLK4	Receptor kinase	0,0356	0,740
AT3G14840.2 LIK1	Receptor kinase	0,0189	0,736
AT5G16590.1 LRR1	Receptor kinase	0,0018	0,694
AT3G49670.1 BAM2	Receptor kinase	0,0039	0,532
AT1G52290.1 PERK15	Receptor kinase	0,0027	0,527
AT4G11460.2 CRK30	Receptor kinase	0,0153	0,776
AT4G04570.1 CRK40	Receptor kinase	0,0019	0,621
AT3G02880.1 KIN7	Receptor kinase	0,0012	0,413
AT2G18960.1 AHA1	H+ ATPase	0,0179	0,436
AT5G57350.4 AHA3	H+ ATPase	0,0202	0,540
AT3G61430.2 PIP1	Aquaporin	0,0029	0,618
AT1G01620.1 PIP1;3	Aquaporin	0,0162	0,493
AT2G39010.1 PIP2;6	Aquaporin	0,0029	0,450
AT4G35100.2 PIP3	Aquaporin	0,0036	0,398
AT2G37170.1 PIP2;2	Aquaporin	0,0058	0,578
AT2G45960.2 PIP1;2	Aquaporin	0,0055	0,362
AT3G53420.2 PIP2;1	Aquaporin	0,0175	0,342
AT1G59870.1 PEN3	ABC transporter	0,0006	0,476
AT1G11260.1 STP1	Sugar transporter 1	0,0016	0,790
AT1G11310.2 MLO2	Calcium channel	0,0296	0,739
AT5G57110.3 ACA8	Calcium ATPase	0,0356	0,380
AT5G42130.1 Mfl1	Iron transporter	0,0006	0,488
AT4G16370.1 OPT3	Iron transporter	0,0172	0,461
AT1G23080.2 PIN7	Auxin transporter	0,0008	0,376
AT2G22500.1 DIC1	Dicarboxylate carrier	< 0,0001	0,363
AT4G26690.1 SHV3	Glycerophosphoryl diester phosphodiesterase-like protein	0,0297	2,258
AT5G55480.1 SVL1	Glycerophosphoryl diester phosphodiesterase activity	0,0029	0,475
AT4G00300.1 nosymbolavailable	Glycosyltransferase activity	< 0,0001	1,348
AT1G05150.1 nosymbolavailable	Glycosyltransferase activity	0,0029	1,224
AT2G32450.1 nosymbolavailable	Glycosyltransferase activity	< 0,0001	0,530
AT2G31960.4 IGSL03	Glycosyltransferase activity	0,0008	0,502
AT4G03550.1 PMR4	Glycosyltransferase activity	0,0035	0,475
AT4G21940.3 ICPK15	Cadium dependent protein kinase	0,0004	1,121
AT2G27600.1 SKD1	ATP hydrolysis activity	0,0037	0,488
ATMG00220.1 COB	Reductase activity	0,0208	0,947
AT2G31110.1 TBL40	O-acetyltransferase activity	0,0011	0,538
AT1G02930.2 IGST1	Glutathione-S-transferase	0,0447	0,721
AT4G35470.2 PIRL4	Intracellular signal transduction	0,0004	0,651
AT5G45750.1 RABA 1c	GTPase activity	0,0036	0,370
AT3G63260.2 MRK1	Kinase activity	0,0018	0,367
AT1G70320.1 UPL2	Ubiquitin protein ligaes activity	0,0055	0,356
AT3G62010.2 nosymbolavailable	Phosphatase activity	0,0055	0,428
AT3G48090.1 EDS1	Lipase activity	0,0013	0,428
AT3G47390.2 PHS1	Hydrolase activity	0,0006	0,426
AT4G30440.1 IGAE1	UDP-glucuronate 4-epimerase activity	0,0110	0,421
AT1G30470.3 nosymbolavailable	Phosphoprotein phosphatase activity	0,0001	0,408
AT1G12360.1 SEC11	Syntaxin binding	0,0092	0,610
AT4G37860.2 nosymbolavailable	DNA binding	0,0079	1,029
AT2G03820.1 NMD3	mRNA binding	< 0,0001	0,527
AT5G09510.1 US19X	mRNA binding	0,0310	0,638
AT2G33410.1 RBGD2	mRNA bbinding	0,0499	0,469
AT1G73720.1 SMU1	RNA splicing	0,0036	0,549
AT5G22440.2 ULX1	RNA binding	0,0388	0,541
AT2G19520.1 MSI4	Histone binding	0,0005	0,336
AT1G12770.2 ISE1	Cell-to-cell mobile RNA	0,0004	0,701
AT4G16180.2 nosymbolavailable	unknwon	0,0001	0,326
AT1G33170.1 nosymbolavailable	unknown	0,0001	0,937
AT1G75460.1 nosymbolavailable	unknwon	0,0107	0,389
AT4G28740.1 nosymbolavailable	unknown	0,0001	0,645
AT1G66240.1 IATX1	unknown	0,0174	0,484
AT3G17900.2 ITRIPP	unknown	< 0,0001	0,343
AT5G15320.2 nosymbolavailable	unknown	0,0302	0,515

Figure S4: FER interactors detected by Co-IP MS/MS. (A) Vulcano plot of detected FER-GFP interactors. Significantly enriched proteins (FDR=0.05 and fold change (FER-GFP/Lti6b-GFP) >2) are marked with colored circles according to the legend. Non-significant proteins are colored grey. (B) List of significant FER-GFP interactors compared to Lti6b-GFP control. Data was obtained from biological triplicates for FER-GFP and biological quadruplets for Lti6b-GFP.

A

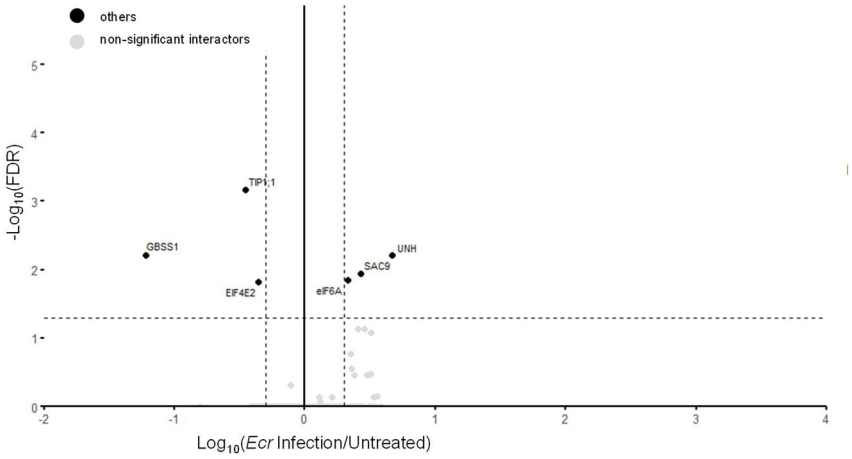

B

Identifier	Molecular function	FDR	log10(fold change)
AT1G32900.1 |GBSS1	Glycosyltransferase	0,0062	-1,223
AT2G36830.1 |TIP1;1	Water channel	0,0007	-0,459
AT3G59770.2 |SAC9	Phosphatase activity	0,0114	0,425
AT4G02030.1 |UNH	Protein binding	0,0062	0,668
AT5G35620.3 |EIF4E2	Translation initiation factor	0,0150	-0,354
AT3G55620.1 |eIF6A	Translation initiation factor	0,0142	0,330

Figure S5: Powdery mildew dependent FER interactors detected by Co-IP MS/MS. (A) Vulcano plot of detected FER-GFP interactors after *Ecr* infection (1 dpi). Significantly enriched proteins (FDR=0.05 and fold change (*Ecr* infection (1dpi)/Untreated) >2) are marked in black. Non-significant proteins are colored grey. (B) List of significant FER-GFP interactors at 1 dpi with *Ecr*, compared to the untreated FER-GFP control. Data was obtained from biological triplicates for each treatment.

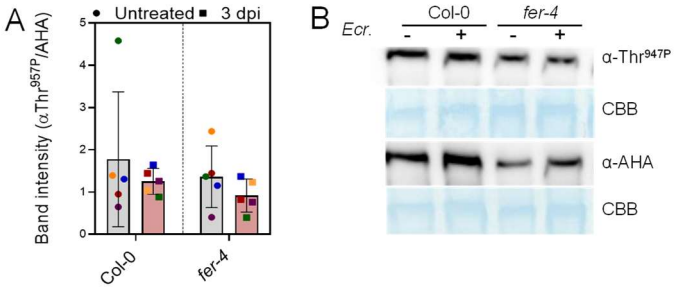

Figure S6: AHA-Thr947 phosphorylation status during powdery mildew infection. (A) Quantification of the band intensities detected in western blot probed with α-AHA and α-Thr^{947P} antibodies. Band intensities were measured using Image J software. Data points indicate individual experiments. Data points from the same experiment are marked with the same color. (B) AHA phosphorylation upon infection with *Ecr* (3 dpi). Western blots were probed with α-AHA and α-Thr^{947P} antibodies. CBB = Coomassie brilliant blue. The experiment was repeated at least three times with similar results.

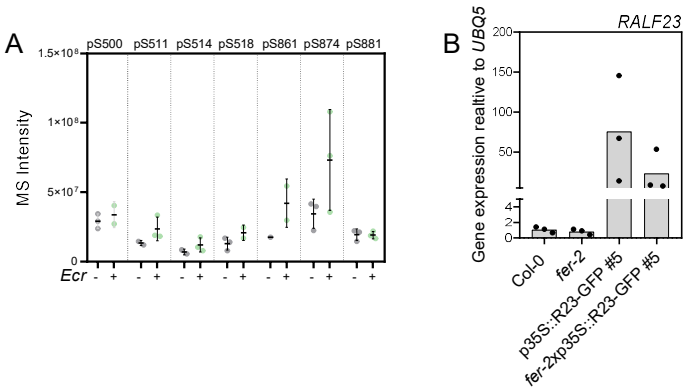

Figure S7: Phosphorylation changes on FER-GFP upon *Ecr* infection and characterization of RALF23-GFP overexpression in Col-0 and *fer-2.* (A) MS Intensities of phosphorylated FER peptides after GFP co-immunoprecipitation of FER-GFP (Untreated and 1 dpi). Mean ± SD, n=3, missing data points occur from missed identification in the LC-MS/MS measurement. (B) RT-qPCR of *RALF23* in untreated adult leaves of the indicated plant lines. Housekeeping gene *UBQ5*. n=3, data points indicate independent biological replicates. A) The data was obtained from biological triplicates for both treatments. B) The experiment was done three times with similar results.

Figure S8: Images of all plant lines used in this study. (A) Representative images of 5 week-old plants used in this study.

1452 **Tables**

1453 **Table S1: Identification of RALF-like peptides from phytopathogenic fungi** [a]species reported to be
1454 able to infect *Arabidopsis thaliana*.

Species	Significant hits in predicted proteins (E-values < $10e^{-05}$)	Significant hits in translated genome assembly (E-values < $10e^{-05}$)	GenBank assembly accession number	Reference
Fusarium oxysporum NRRL 32931	1	2	GCA_000271745.2	(Delulio et al., 2018)
Pyrenophora tritici-repentis Pt-1C-BFP	1	1	GCA_000149985.1	(Manning et al., 2013)
Golovinomyces cichoracearum[a] UMSG1	0	0	GCA_003611235.1	(Wu et al., 2018)
Erysiphe neolycopersicum[a] UMSG2	0	0	GCA_003610855	(Wu et al., 2018)
Erysiphe necator EnFRAME01	0	0	GCA_024703715.1	(Zaccaron et al., 2023)
Blumeria graminis f.sp. *tritici* CHE_96224	0	0	GCA_900519115.1	(Müller et al., 2019)
Podosphera xanthii YZU573	0	0	GCA_028751805.1	(Xu and Chen, 2023)

1455

1456

1457 **Table S2: Plant lines used in this study.**

Plant line	Genetic Backgorund	Reference
fer-4	Col-0	(Duan et al., 2010)
fer-2	Col-0	(Deslauriers and Larsen, 2010)
pFER::FER-GFP	*fer-4*	(Duan et al., 2010)
llg1-2	Col-0	(Li et al., 2015)
llg1-3	Col-0	(Shen et al., 2017)
lrx1/2/3	Col-0	(Draeger et al., 2015)
lrx1/2/3/4/5	Col-0	(Herger et al., 2020)
p35S::LRR4-citrine	Col-0	(Fabrice et al., 2018)
ralf1/22/23/31	Col-0	(Lan et al., 2023)
CRISPR *ralf3x*	Col-0	Generated in this study
CRISPR *ralf7x*	Col-0	Generated in this study
p35S::RALF23	CRISPR *ralf7x*	Generated in this study
p35S::RALF23$^{Y93A/Y96A}$	CRISPR *ralf7x*	Generated in this study
p35S::RALF23$^{Y113A/Y114A}$	CRISPR *ralf7x*	Generated in this study
mlo2/6/12	Col-0	(Consonni et al., 2006)
CRISPR *myc2*	*fer-4*	Generated in this study
PMEI3-OE	Col-0	(Peaucelle et al., 2008)
ost2-2D	Col-0	(Merlot et al., 2007)
pme3	Col-0	(Guénin et al., 2011)
pme17	Col-0	(Del Corpo et al., 2020)
pUBQ10::SYP122-pHusion	Col-0	(Kesten et al., 2019)
pUBQ10::SYP122-pHusion/CRISPR *fer*	pUBQ10::SYP122-pHusion	Generated in this study
pFER:FER-GFP	*fer-4*	(Chakravorty et al., 2018)
pFER:FER^{K565R}-GFP	*fer-4*	(Chakravorty et al., 2018)
p35S::RALF23-GFP	Col-0	(Dobón et al., 2015)
fer-2 x p35S::RALF23-GFP	*fer-2*	(Stegmann et al., 2017)
pFER:FER^{WT}-GFP	*fer-4*	(Xiao et al., 2019)
pFER:FER^{N303Y}-GFP	*fer-4*	(Xiao et al., 2019)
pFER:FER^{G257A}-GFP	*fer-4*	(Xiao et al., 2019)
p35S::Lti6b-GFP	Col-0	(Kadota et al., 2014)

1458

1459

1460 **Table S3: Primers used in this study**

Primers used for cloning		
Name	**Sequence (5' - 3')**	**Purpose**
RALF23_Esp3I_F	ttCGTCTCaaatgagaggactctccagaaac	p35S::RALF23
RALF23_Esp3I_R	ttCGTCTCaactatgagcgccggcagcgag	
R23^{Y113AY114A}_F	ttCGTCTCctgccgccaattgtcgacgtg	p35S::RALF23$^{Y113A/Y1114A}$
R23^{Y113AY114A}_R	ttCGTCTCcggcagatgcgccgcgacgtg	
R23^{Y93AY96A}_F	ttCGTCTCatcagcgctggtgcgctgaggag	p35S::RALF23$^{Y93A/Y96A}$
R23^{Y93AY96A}_R	ttCGTCTCgctgatgtacctcctcgtagc	
MLO2_Esp3I_F	ttCGTCTCaaatggcagatcaagtaaaag	p35S::MLO2-mCherry
MLO2_Blunt_R	tttcttaaaagaaaaatctcttaa (5'Phosphorylated)	
Primers used RT-qPCR		
Name	**Sequence (5' - 3')**	**Purpose**
Ath_Rubisco_F	TGATGGACGGTACTGGACAA	Quantification of plant DNA
Ath_Rubsico_R	GAAGCTTGGTGGCTTGTAGG	
Ecr_Tubulin_F	TGACAGCCCGGAATGAGT	Quantification of fungal DNA
Ecr_Tubulin_R	TTGTCTTCGTTTCCCAGGTC	
RALF23_qPCR_F	TTCATAACTGGTCCGTCGCC	RALF23
RALF23_qPCR_R	AGCTAATATGCGCCGGTTGA	
UBQ5_qPCR_F	ACTCCTTCCTCAAACGCTGA	UBQ5
UBQ5_qPCR_R	CCAAGCCGAAGAAGATCAAG	
MYC2_qPCR_F	GTGCGGGATTAGCTGGTAAA	MYC2
MYC2_qPCR_R	ATGCATCCCAAACACTCCTC	
PR1_qPCR_F	CGGAGCTACGCAGAACAACT	PR1
PR1_qPCR_R	CAGACAAGTCACCGCTACCC	
JAZ10_qPCR_F	GAGAAGCGCAAGGAGAGATTAG	JAZ10
JAZ10_qPCR_R	CTTAGTAGGTAACGTAATCTCC	
PDF1.2_qPCR_F	CTG CTT TCG ACG CAC CGG CA	PDF1.2
PDF1.2_qPCR_R	TGA TCC ATG TTT GGC TCC TTC	
Primers used for genotyping		
Name	**Sequence (5' - 3')**	**Purpose**
GG pUC18 Seq-F	GTATCACGAGGCCCTTTCGT	Inserts in GoldenGate pUC18
GG pUC18 Seq-R	TAATGAATCGGCCAACGC	
pGGPlant-XL-AB-insert_Fwd	AAACGACAATCTGAGCTCCACC	Insert in GoldenGate pGGPlantXL-AB
pGGPlantXL-AB-insert_Rev	CGGTGTCATCTATGTTACTAGAT	
RALF1_F	CAAAATTAAAAAATCGAGTCCAC	CRISPR RALF1
RALF1_R	GCTTGATGGATCAAAGAAAAC	
RALF14_F	GCTCTTAATCTTCGCCG	CRISPR RALF14
RALF14_R	GTAAACCGGTAACAATGTG	
RALF18_F	CATCACAAACCATTTCAACG	CRISPR RALF18
RALF18_R	CACACCAACGAAAGGAAG	
RALF22_F	GTTTCCAAGAGAGAAAGAGAG	CRISPR RALF22
RALF22_R	GAAAATCGAGAAGAGAGACAG	
RALF23_F	CTTCATAGTTCGTGCACAG	CRISPR RALF23
RALF23_R	CTAATAATCCGCAATGAACTTAG	
RALF31_F	CTTCTTCTGCTTAGAGACAG	CRISPR RALF31
RALF31_R	CAGCAATGCAAAAGCTTAATC	
RALF33_F	CCTCAGAGAAAGAAGAAGAAAG	CRISPR RALF33
RALF33_R	GCAATGCAAAGTATAAACATAG	
RALF34_F	CCTCTTTACATGTGACTTCC	CRISPR RALF34
RALF34_R	CACGGTTTACAAACAAACATC	
MYC2_F	GGAACACACGAAGGTTGGAC	CRISPR MYC2
MYC2_R	CTGCTACTTCTTTCACGACGG	
FER_F	CGTAACCAAACGAACATG	CRISPR FER
FER_R	GGTAAGTGAAACCAGAGTC	

1461

1462

1463 **Table S4: CRISPR target sites**

Target site	Sequence	Purpose
RALF1.1	ACACTCTGCTATTGAACCG	Generation of CRISPR *ralf* mutants
RALF1.2	AATTGTCAGAACGGAGCTC	
RALF14.1	GATGCATTTTCCACTCAAC	
RALF18.1	GTGGTTGCAGTGCCGCTAC	
RALF22.1	GTTCGATTCAGACATAAGC	
RALF22.2	CGTACTACAACTGCCAGCG	
RALF23.1	CCTCGTAGCTAATATGCGC	
RALF23.2	CAGCCACGAGAGTAAGGAT	
RALF31.1	TGGCGCAGAAACGGTACAT	
RALF31.2	TTTGTGTCTCTAGCGCATC	
RALF33.1	CGATCGAGTCGAAATGCAA	
RALF33.2	TAGCGCTATTACTCGTTGC	
RALF34.1	CTCTCACTCTTCTACCCGA	
RALF34.2	CCGTTCATCCGTATAGCCG	
MYC2.1	CCGCCGGAGTAGAAAACGG	Generation of *fer*-4 CRISPR *myc2*
FER.1	GACGATTAAGTATCCTACG	Generation of pUBQ10::SYP122-apopHusion CRISPR *fer*-4
FER.2	TGATCGATGAAGATCACAG	

1464